VAPORIZATION OF THIN LIQUID FILMS

Donald Kenneth MacKenzie

NAVAL POSTGRADUATE SCHOOL
Monterey, California

THESIS

VAPORIZATION OF THIN LIQUID FILMS

by

Donald Kenneth MacKenzie

Thesis Advisor: P. J. Marto

December 1972

Vaporization of Thin Liquid Films

by

Donald Kenneth MacKenzie
Lieutenant, United States Navy
B.S., Tufts University, 1966

Submitted in partial fulfillment of the
requirements for the degree of

MASTER OF SCIENCE IN MECHANICAL ENGINEERING

from the

NAVAL POSTGRADUATE SCHOOL
December 1972

ABSTRACT

Experimental results are presented for saturated nucleate pool boiling of distilled water and ethyl-alcohol from 1-7/8" diameter Nickel disks with pool depths from 1.0 inch to a thin film of 0.015 inch. Experimental runs were conducted on a mirrorlike surface utilizing distilled water and ethyl-alcohol; on a grooved surface with distilled water as the working fluid; and on a surface covered with 4 layers of Nickel 50 x 40 mesh with distilled water as the working fluid.

Results show that liquid level has little effect on the heat transfer coefficient above a level of 0.2 inch on all three test surfaces; however, below 0.2 inch a rapid increase in the heat transfer coefficient occurs with the lowering of the liquid level. Two types of thin film dryout were noted on the mirrorlike surface: dryout under a dome and dryout in absence of a dome. A grooved surface appears to provide a means of obtaining a stable high heat transfer coefficient at liquid films as thin as 0.015 inch.

TABLE OF CONTENTS

LIST OF TABLES

LIST OF FIGURES

ACKNOWLEDGEMENT

The author would like to express his sincere appreciation and gratitude to Dr. Paul J. Marto of the Naval Postgraduate School for his continual advice, encouragement, interest, and constructive criticism of the work as thesis advisor.

Many thanks are due to several people whose helpful interest and technical advice contributed much to the successful operation of the apparatus, especially to Mr. George Baxter of the Mechanical Engineering Machine Shop who constructed the test apparatus.

Also many thanks to my wife, June, for her patience, understanding, encouragement, and valuable assistance in reducing the data and in typing the rough copy.

I. INTRODUCTION

A. BACKGROUND

Since the advent of the space age numerous investigations into the theory and applications of heat pipes have been conducted. Although noted by Gaugler in 1942 [1], the relatively simple principle of heat pipes did not come into its own right until 1964 with the studies of Grover, et al. [2]. In general, a heat pipe consists of a closed cylindrical container in which vaporization and condensation of a fluid takes place. A porous wick material lines the container while maintaining a vapor space in the center. Heat added at one end of the container causes evaporation of saturated liquid in the wick. The vapors then travel through the center space to the heat sink where the vapor condenses in the wick. The resulting condensate is returned to the heated end of the container by the action of capillary forces in the liquid layer and the cycle continues. Heat pipes are potentially inexpensive heat transfer devices which can operate at high heat fluxes, have no moving parts, are independent of gravity, require no maintenance, and operate silently and reliably for extended periods of time.

Garg [3] conducted an investigation of heat pipe technology for Naval applications. He concludes that heat pipes may be useful for a wide range of Naval applications because of the properties cited above. Also contributing to Naval application are their compactness and light weight for a given use when

compared to conventional heat dissipation devices; their flexibility in configuration, which can be used to transfer heat to or from otherwise inaccessible locations; and their ability to maintain a constant temperature over a large surface at varying power levels. At the present time, space application remains the main area in which heat pipes are being utilized; however, Garg points out that several of the Naval laboratories are looking at the heat pipe for utility type applications although no work in this area has commenced. A couple of the uses suggested by Garg for Naval application are:

1) Heat pipes could be used to protect the refractory walls of boilers.

2) Cooling of large power transformers could be carried out more effectively by using heat pipes in place of the presently used radiators.

3) Heat pipes could be efficiently used where heat is to be removed from or added to high voltage or high radiation areas or spaces.

Heat pipes have been operated using various temperatures, pressures, wicking materials and fluids [4]. Studies have shown that the heat pipe performance is mainly limited by the wick resistance of the capillary structure when using ordinary fluids. When the capillary action is exceeded the supply of working fluid to the evaporator is insufficient and dryout occurs in the evaporator causing failure of the pipe. Nucleate boiling may also occur in the wick structure leading perhaps, to dryout.

The mechanisms of evaporator heat transfer in a heat pipe have received considerable attention. Alleavitch [5] designed an apparatus which would simulate the vaporization zone of a heat pipe in order to study this heat transfer mechanism. Ferrell and Johnson [6] reported their results of an experimental investigation of the mechanism of heat transfer during the evaporation of a fluid in a porous wick structure in contact with a heated surface. Seban and Abhat [7] investigated evaporator heat transfer from screen wicks. Marto and Mosteller [8] studied the effect of nucleate boiling on the operation of low temperature heat pipes, and its effect on the mechanism of evaporator heat transfer. Gregory [9] investigated nucleate boiling from a mesh covered surface simulating a heat pipe.

Since heat pipes operate at low liquid levels, it is appropriate that an investigation of nucleate boiling at low liquid levels be made. Previous attention toward this area of nucleate boiling has been small, with the majority of studies on nucleate boiling being made from a surface situated well below the liquid surface. Nishikawa, et al. [10] investigated nucleate boiling at liquid levels from 1 mm to 30 mm on several flat horizontal surfaces using various working fluids. They suggest that a critical layer thickness exists below which dryout will always occur. Patten and Turmeau [11] conducted heat transfer experiments from a flat horizontal surface covered by liquid layers from 5 mm to 0.5 mm

and proposed mechanisms for nucleate boiling in thin liquid layers which differ from normal pool boiling.

B. THESIS OBJECTIVE

The objective of this study was to systematically investigate nucleate boiling at low liquid levels on a flat horizontal surface, and to determine what effect test surface conditions have upon thin film boiling.

II. EXPERIMENTAL DESIGN

A. FACTORS CONSIDERED AND CHOICE OF MATERIALS

The overall design of the boiling apparatus used in this study was largely influenced by the requirements to allow the condensate to return directly into the boiling area, and to allow close monitoring of the liquid level in the boiling area. While striving to satisfy the above requirements, other factors were kept constantly in mind. Some of these factors included: permitting visual observation of the boiling process, flexibility of operation, simplicity in design and construction, as well as safe operation of the system.

The final design was quite similar to that used by Gregory [9]. In fact, several of his components or design ideas were used with some modifications. The final design consisted of two major components: a test surface/heater assembly which contained a nickel cylinder to boil from and the necessary heater elements to provide the required heat fluxes; a glass condenser assembly which provided a medium to hold the test fluid and to permit the passage of external coolants. These components will be described in detail in the following section.

Previous studies of heat pipe operation at the Naval Postgraduate School [9] and several studies during the period of this report, had used nickel pipe with nickel screen serving as the wicking material and for this reason, a nickel boiler surface was used. Nickel screen, fed by gravity,

was used as the wicking material in some runs because of its ease of fabrication, dimensional stability, thermal conductivity, and wetting properties as recommended by Kunz, et al. [12].

With the exception of the nickel and electric resistance heaters, all materials used in this experiment were readily available and were used for simplicity of construction as well as to avoid risk of corrosion and contamination of the boiling fluids - distilled water and ethyl alcohol. Figure 1 is a cross-sectional view of the boiling apparatus, and Figure 2 an overall view of the experimental apparatus.

B. COMPONENTS

The two nickel cylinders used by Gregory [9] were modified for use in this experiment. Originally the nickel cylinder was machined from a 2 1/2 inch Nickel 200 rod to a 1.875 inch diameter with a 0.1875 inch lip, 0.050 inch thick, extending from the sides of the cylinder, 0.010 inch from the boiling surface itself. The lip was undercut until the final thickness at the machined diameter of the cylinder was 0.015 inches. Modification included the leveling of the boiling surface to the lip and the shortening of the overall height to 2" from 2 1/4" with the bottom 0.25 inch threaded. The bottom of the lip provided a means of supporting the heater-boiling surface assembly from the phenolic base while the undercutting reduced the extent of conduction losses through the lip.

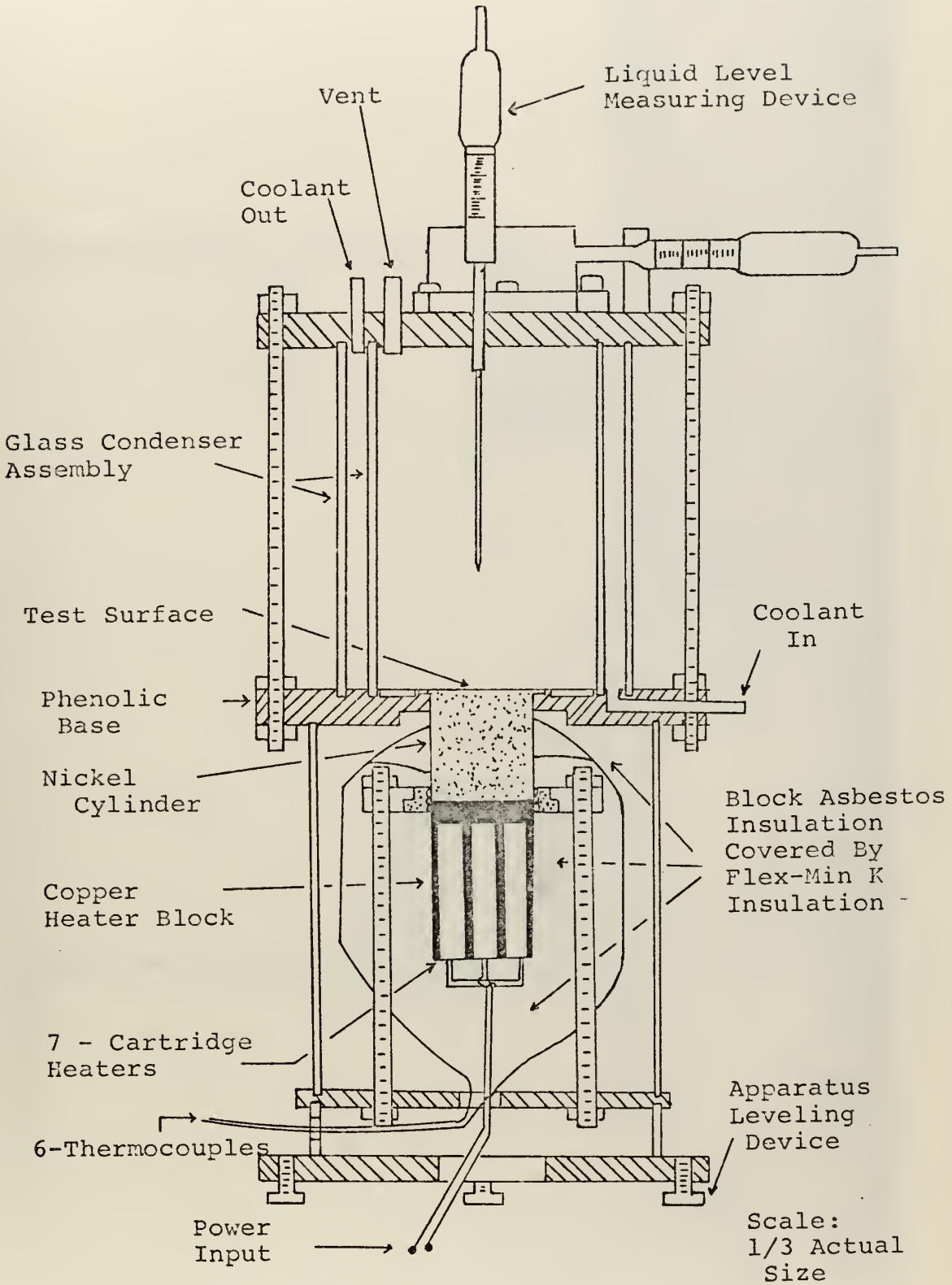

Figure 1. Cross Sectional View Boiling Apparatus

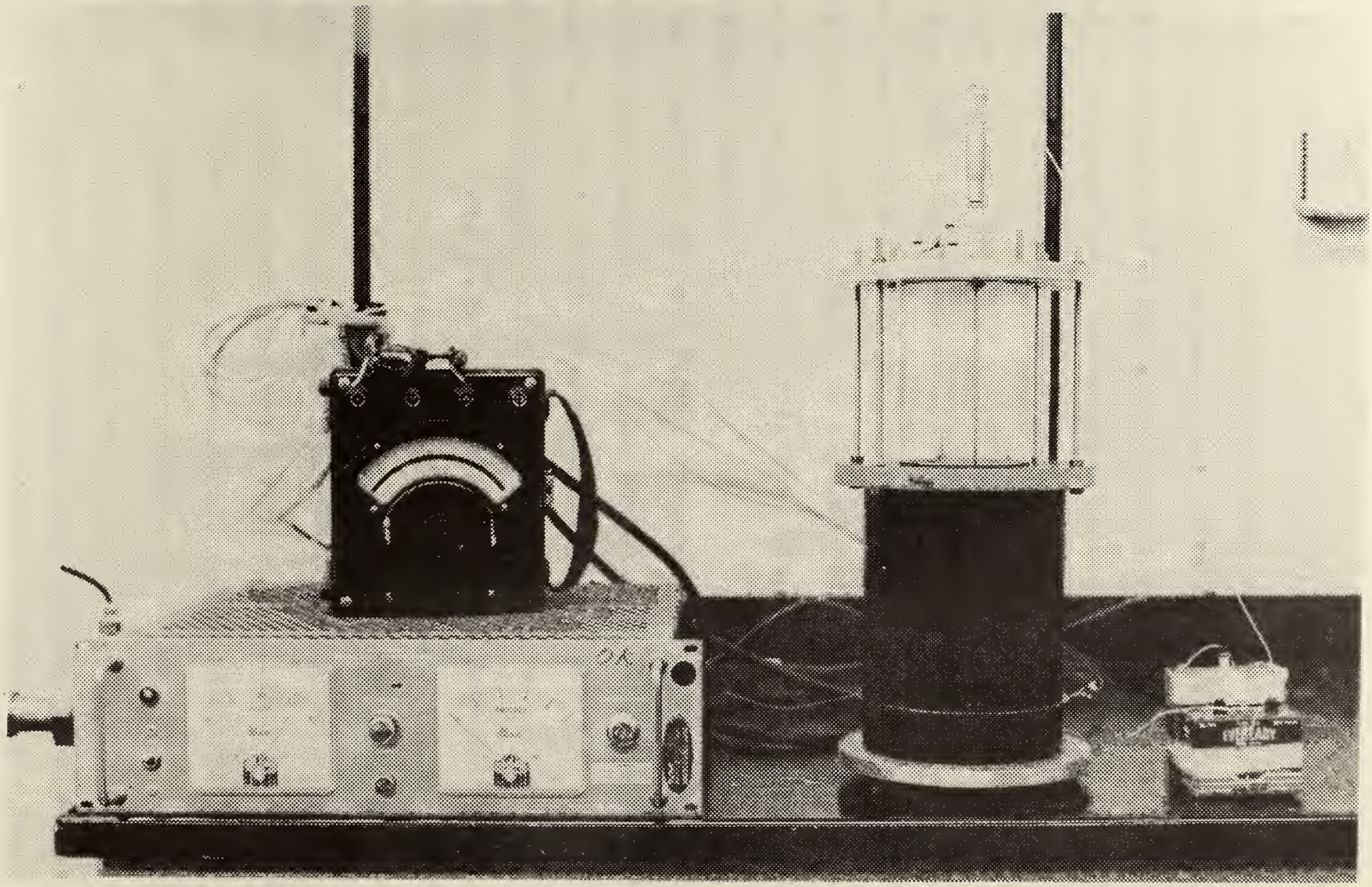

Figure 2. Overall View of Experimental Apparatus

Six thermocouple wells, 0.041 inch diameter, were drilled at a number of axial and radial positions in the nickel cylinder to accommodate the thermocouples. Four of these wells were drilled at ninety degree angles to each other, .500 inch below the boiling surface to a depth of .625". The fifth hole was drilled 1.000 inch below the surface and the last hole was drilled 1.500 inch below the surface, both to a depth of .625". No two holes lay in the same plane parallel with the longitudinal axis of the cylinder. The first four were placed in a plane perpendicular to the axis to determine if the temperature distribution throughout the nickel was uniform.

As a support for the nickel cylinder and as a base for the boiling apparatus a 8.5 inch phenolic disk 5/8" thick was chosen for its low thermal conductivity, low porosity, and high machinability. The 1.875 inch hole in the center was counterbored 0.050 inch to a radius of 1.125 inch so that the actual boiling surface would sit flush with the phenolic surface and was counterbored on the bottom .250 inch to a radius of 1.562" to accommodate the thermocouples. A place for the nickel screen ring was counterbored .125 inch from a 1.250" - 1.437" radius on the phenolic dish. Grooves were cut .1875" in the disk to accommodate both the inner and outer glass fluid containers along with their 'O' ring sealant.

The 3-inch high copper heater unit, chosen for its high thermal conductivity, was machined to a diameter of 1.875

inches, threaded at the top and had seven 0.375 inch holes, 2.250 inches deep, drilled into the bottom. Watlow Firerod Cartridge Heaters, 0.375 inch in diameter, 2.250 inches long and having a capacity of 250 watts each, were inserted into the holes. The bottom surface of the nickel cylinder and the top surfaces of the copper were polished until uniform, then coated with Silver Goop to ensure good contact and to prevent sticking after heating. A threaded nickel ring held the two cylinders in direct contact. A stainless steel collar was attached to this nickel ring to which 6 hold down bolts were attached to form a sealant between the nickel boiling surface and the phenolic base. (Figure 1)

After assembly, the cylinders were covered with 1-inch thick asbestos preformed insulation which was covered by several layers of Flex - Min K asbestos insulation. The lower portion of the apparatus, i.e. cylinders and insulation, was contained in a 6 1/4" diameter stainless steel container mounted on top of a leveling device which consisted of a bottom plate with 3 jacking screws attached, a 1-inch high stand and a hold down plate for bolting down the nickel cylinders and copper heating assembly. Two level indicators were mounted on the phenolic support for the nickel cylinder which, along with the jacking screws, provided a means of leveling the boiling surface.

The condenser assembly consisted of inner and outer fluid containers cut from 6" high glass tubes; 4.140 inches in

diameter by .110 inches thick, and 5.290 inches in diameter by .130 inches thick respectively. An aluminum top cap, 8 1/2" in diameter, 7/16" thick was placed on top of the glass condenser assembly. A rubber gasket formed a sealant at the top and bottom of the assembly. If a coolant was used, the fluid entered the glass condenser through a hole in the phenolic base and left through a hole in the aluminum cap. The boiling fluid entered the boiling area through a hole in the aluminum cap and could be removed through this hole with an eyedropper during the constant heat flux experimental runs. Six bolts provided a means of sealing the top cap, glass condenser assembly, and phenolic disk together.

C. INSTRUMENTATION

Temperature measurements were made with copper-constantan thermocouples using a distilled water-ice bath as a reference. A total of six thermocouples were used to measure the temperature profile in the nickel cylinder, while one thermocouple was used to monitor the fluid temperature. Thermocouple output was measured with a Hewlett-Packard 2010C Data Acquisition System containing an integrating digital voltmeter and guarded data amplifier. Thermocouple selection was provided within the DA system. This instrument gave a printed digital output with an accuracy of $\pm$ 0.5 microvolts.

Heat flux control was provided initially by means of a variac to regulate the voltage input along with a voltmeter

and ammeter to monitor power input. A D.C. regulated power supply was later used to provide this control.

A micrometer fluid level indicator was mounted on the aluminum cap which permitted measuring of the liquid level directly over the center of the boiling surface and radially outward to 1.125 inches. This device consisted of two micrometers mounted in an aluminum block. One micrometer, mounted horizontally, measured the radial distance while the other micrometer, mounted vertically, measured the liquid level with its probe. An electrical circuit between the vertical micrometer and test surface would close and activate a light when the probe made contact with the test fluid, signalling the point to read the micrometer which measured the liquid level.

III. EXPERIMENTAL PROCEDURE

A. PREPARATION OF TEST SURFACES

Throughout this research work the condition of the test surface had to be known in order to compare results for reproducibility. No theoretical nor experimental method exists today which can predict the number of active sites of a given size on a test surface which has undergone a prescribed polishing procedure. However it is hoped that the structure of a given test surface may be adequately defined if an accurate description is given of the polishing procedure used in preparing the surface [13]. Much time was consumed in preparing the boiling surface as explained in the following paragraphs.

1. Mirrorlike Finish

In the majority of tests a mirrorlike finish was required. In order to obtain this finish, great care had to be maintained at all times. Rough polishing was done on a Buehler Metallurgical Manual Grinder. This grinder contained strips of 0 emery polishing paper which were placed over rectangular glass plates and held in place by clamps. The test surface was placed face down on the 0 emery paper and was stroked over the paper in one direction only, until all the original scratches were removed. This required approximately 200 strokes and several changes of the polishing paper. The test surface was then rotated 90 degrees and was carefully stroked in this direction over the 2/0 emery

polishing paper until all the scratches left from the 0 emery polishing paper were removed. Upon completion of the rough polishing, the surface had a high gloss finish although there were still many visible scratches.

The test surface was then cleaned in an ultrasonic cleaner, which helps to wash out small dust particles and bits of metal trapped in the cavities on the surface. This was followed by washing with an alcohol jet and drying with a hot air jet. It was then put on the No. 6 diamond compound wheel (6 microns). It is important that the diamond compound be put on the center area of the grinding wheel and be diluted by alcohol before starting the grinding operation. The test surface was rotated 90 degrees and was held gently near the edge area of the wheel. Alcohol was constantly injected on the wheel cloth. Operation was continued until the scratches due to the 2/0 emery polishing paper disappeared completely. The test surface was then cleaned again, and put on the No. 3 diamond compound wheel (3 microns) with a 90 degree rotation. The process continued to a No. 1 diamond compound (1 micron) wheel. During the last few minutes of grinding process on the No. 1 wheel, the test surface was placed near the center part of the wheel where the rubbing speed is lower, and a heavier pressure was applied. After a few minutes the surface would become shining, mirrorlike smooth. It was once more washed in an ultrasonic cleaner, alcohol jet, and hot air jet. The surface was then carefully covered with masking tape until ready for use.

If refinishing was desired after an experimental run(s) the above process was repeated starting with the #3 diamond wheel, and continued through the #1 diamond wheel. Table 1 indicates when refinishing was accomplished prior to a run.

2. Grooved Surface

Experimental runs 32 through 36 required grooves in the test surface. This was accomplished by machining the same nickel cylinder as used in runs 1 through 27 with a .008" mill saw, to a depth of .006" with a nominal 62 grooves per inch. Figure 3 shows a top view and side view of the finished test surface. After machining, the surface was cleaned in an ultrasonic cleaner, followed by rinsing in distilled water, alcohol, and reagent grade acetone and finally dried in a hot-air jet.

3. Mesh Covered Surface

Experimental runs 36 and 37 required wire mesh to be sintered to the test surface. Four layers of nickel, 40 x 50 wire mesh screen, were sintered to the surface of the nickel test surface used in runs 28 - 31, in a Watkins Johnson hydrogen controlled atmosphere furnace for two hours at 1200°C. The wire size was 0.009 inches, with a percent open area of 35.3. Thickness of the 4 layers after sintering was .081 inches.

Prior to sintering, the wire mesh was prepared as follows. The pieces were cut to a diameter of 2 1/4 inches

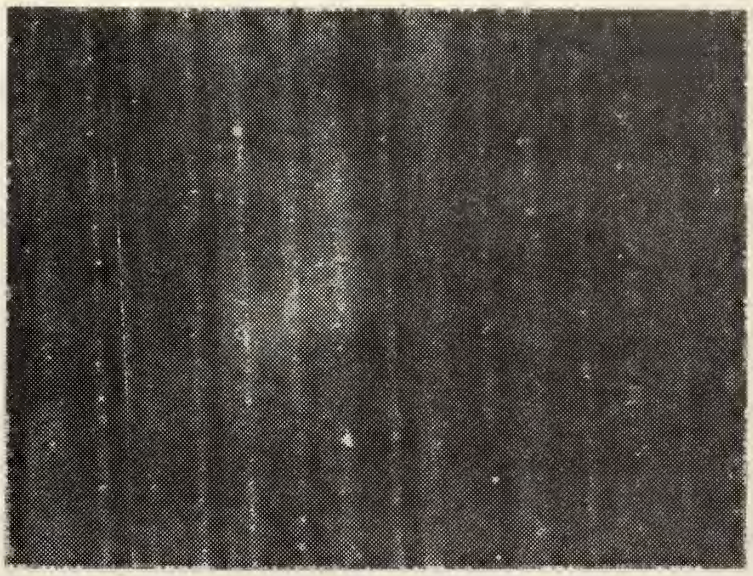

Top View (Approx. 30 X)

Side View (Approx. 30 X)

Figure 3. Photograph of Grooved Test Surface

and cleaned in an ultrasonic cleaner, followed by rinsing in distilled water, alcohol, and reagent grade acetone. This prepared the samples for thermal oxidation as recommended by Kunz, et al. [12]. Thermal oxidation was accomplished by placing the screen pieces in a Lindberg Hevi-duty Electric Furnace for two hours at a temperature of 500°F. Thermal oxidation results in the formation of nickel oxide on the screen which, having a smaller contact angle than pure nickel, increases the wettability of the nickel screen.

Since the lip of the test surface used in the sintering process had previously been damaged, it was decided to sinter the mesh over the center 1.8 inch diameter of the test surface, and allow the rest of the 2 1/4 diameter screen pieces to rest on the lip area only. A special clamping device was made from an asbestos ceramic material and Nichrome wire, which applied pressure over the sintering surface. Care was taken to orient the screen relative to the mesh opening; however, during the sintering process the mesh slipped, resulting in no specific screen orientation during the runs with the sintered surface. Other than washing the surface with acetone, no special preparation was done on the nickel surface prior to sintering the screen to it.

B. PREPARATION OF EQUIPMENT

Once the test surface was prepared, assembly of the boiling apparatus proceeded. All parts which came into contact with the test surface or test fluid were thoroughly

cleaned and degreased. This process consisted of using Trichloroethylene for degreasing, followed by a detergent washing, a distilled water rinse and a final rinse with reagent grade acetone.

The assembly process consisted of assembling the lower section of the boiling apparatus followed by a check of the voltmeter and ammeter for proper connections, operation and zero readings. The thermocouples in the nickel cylinder were then checked by applying an input of 25 volts and reading the Data Acquisition System. Throughout the data collection process, the Data Acquisition System was left operating to prevent any malfunction caused by repeated start-up and securing. As a result, only a minor calibration, zeroing of the apparatus, was required prior to each run. If the instrumentation checked out, the top section of the boiling apparatus was assembled and checked for leaks. Any external leaks were corrected using a silicone rubber sealant, while internal leaks required disassembly of the top section to investigate the cause. Changing of the test surface required the above procedure to be repeated. Prior to the beginning of any experimental run the leveling device was checked to insure a level test surface.

C. NORMAL OPERATIONS

1. Constant Liquid Level

The system was prepared for experimental runs by introducing sufficient test fluid into the test area to

bring the level up to the desired value. The level in the test area was monitored by the liquid level device mounted on the top aluminum cap for levels below 2" and by means of a ruler for levels over 2". A heat flux corresponding to a 40 volt input (approximately 180 watts) was added and the test fluid was allowed to boil for 30 minutes in order to degas the fluid. Power was then secured and the system allowed to cool until the thermocouple just above the heaters read less than 3.200 millivolts (approximately 170°F). A final check of the fluid level was made and the system was considered ready for operation. Runs 1-3 used tap water as a coolant, while during run 4 an air blower was used to provide coolant for condensing the vapor.

At the start of each run, the atmospheric pressure was recorded from an aneroid barometer and used to calculate the saturation temperature of the test fluid. Voltage was increased in 5-volt increments starting with 25 volts. Data was collected at the 5-volt levels, up to a maximum of 80 volts (approximately 500 watts). At this voltage, the fluid level fluctuated so rapidly, that the system couldn't condense most of the vapor. Data consisted of 6 thermocouple readings in the nickel cylinder, 1 thermocouple reading in the liquid, 1 thermocouple reading in the cooling chamber, the input voltage and input current. Data was obtained when a semi-steady state operation for a given heat flux was reached. Semi-steady state was assumed to be the point at which the

voltage of the thermocouple nearest the heaters was increasing at a rate less than .010 millivolts per minute, which corresponds to a temperature rise rate of approximately .3°F per minute. Between each data point the water level was measured.

Throughout the experimentation the apparatus was monitored closely and significant occurrences and visual observations were noted on the data sheet.

2. Constant Heat Flux

Problems with maintaining the fluid level were encountered at high heat flux during constant liquid level runs requiring the experimental procedure to be modified. Instead of varying the heat flux while maintaining a fixed fluid level, the heat flux was held constant by using a 40 volt DC regulated power supply, and the test fluid level was varied. Fluid levels from 1.00" down to .015" were used in these tests, while constant heat fluxes from 8,000 - 25,000 $Btu/Hr-Ft^2$ were applied. Power to the heater block was adjusted to give the desired heat flux. Steady state conditions were assumed to have been met when there were virtually no fluctuations ($\pm$ .003 MV) in the thermocouple millivolt readings for a period of 30 minutes . Thermocouple readings and the liquid level readings were then recorded. Because condensation formed on the liquid level probe and vapor domes were present on the liquid surface, three readings of the liquid level were taken and the average value recorded on

the data sheet. The liquid level was then reduced to the next desired value, and after conditions stabilized, thermocouple readings and liquid level measurements were again recorded. This process was repeated until dryout occurred on the boiling surface. The power to the heater block was then adjusted to give a new desired heat flux, and more test fluid was added to bring the liquid level to approximately 1.00" and the above process repeated for this heat flux.

D. DATA REDUCTION

The thermocouple millivolt readings, applied current and voltage readings, and atmospheric pressure readings were put into a data reduction program written for an IBM 360 computer. This program calculated the thermocouple temperatures, the heat flux from the power input, and thermocouple temperatures, the conductivity of the nickel cylinder, the saturation temperature, the surface temperature, surface-solution temperature difference as well as plotting graphs of heat flux vs. surface-saturation temperature. Because of the linearity of the temperature distribution in the nickel cylinder the heat flux could be calculated by using Fourier's heat conduction equation:

$$\frac{Q}{A} = -k \frac{\Delta T}{\Delta X} \qquad (1)$$

The surface temperature was determined by extrapolating this lineal temperature distribution to the test surface as explained in Appendix D.

A sample calculation of the data is given in Appendix B, along with an uncertainty analysis in Appendix C.

IV. RESULTS AND DISCUSSION

In all, a total of 37 experimental runs were completed. Table 1 presents a summary of all experimental runs. Results have been divided into 6 categories for discussion purposes:

1) Testing of Experimental Apparatus
2) Aspect of Boiling
3) Reproducibility and Aging Effect
4) Effect of Liquid Level on Heat Transfer Coefficient
5) Vaporization of Liquid Levels Below .200 Inch
6) Special Surfaces to Improve the Heat Transfer Coefficient

A. TESTING OF EXPERIMENTAL APPARATUS

The purpose of Run 1 was to test out the design apparatus and to check the data reduction program. It initially appeared that the apparatus was functioning correctly and that the results obtained were similar to previous studies; however, by the end of Run 3 it was evident that the use of the tap water coolant for condensing purposes prevented constant pool boiling and interfered with the normal pool boiling curve. Figure 4 shows the results of Run 1 and 3. At high heat flux during Run 3 the boiling water circulated in a system, flowing upward in the central part and then flowing downward along the container walls transferring heat in the process. This sub-cooled water flowed inwards toward the test surface which resulted in the change in the normal boiling curve. This problem could have been corrected

TABLE 1

SUMMARY OF EXPERIMENTAL RUNS

Run Number	Test Fluid	Surface/Condition	Constant Water Level/ Heat Flux	Results Shown in Figure No./Comments
1	Dist. Water	#1 - Mirror/Polished	1.5 Inches	4
2	Dist. Water	#1 - Mirror/Repolished	3.0 Inches	Test of Boiling Apparatus
3	Dist. Water	#1 - Mirror/Repolished	2.8 Inches	4
4	Dist. Water	#1 - Mirror/Repolished	3.0 Inches	4
5	Dist. Water	#1 - Mirror/Repolished	.995 Inches	5, 6
6	Dist. Water	#1 - Mirror/Cleaned with Acetone	.495 Inches	6
7	Dist. Water	#1 - Mirror/Repolished	.225 Inches	6
8	Dist. Water	#1 - Mirror/Repolished	16,600 Btu/Hr - Ft^2	Test of Constant Heat Flux Method
9	Dist. Water	#1 - Mirror/Repolished	10,300 Btu/Hr - Ft^2	Test of Constant Heat Flux Method
10	Dist. Water	#1 - Mirror/Repolished	10,300 Btu/Hr - Ft^2	11
11	Dist. Water	#1 - Mirror/14 Hrs.*	14,700 Btu/Hr - Ft^2	12
12	Dist. Water	#1 - Mirror/19 Hrs.	20,200 Btu/Hr - Ft^2	13, 15

*Total Number of Boiling Hours Without Refinishing Surface

SUMMARY OF EXPERIMENTAL RUNS (continued)

Run Number	Test Fluid	Surface/Condition	Constant Water Level/ Heat Flux	Results Shown in Figure No./Comments
13	Dist. Water	#1 - Mirror/24 Hrs	10,000 Btu/Hr - Ft^2	11, 15
14	Dist. Water	#1 - Mirror/31 Hrs	14,200 Btu/Hr - Ft^2	12, 15
15	Dist. Water	#1 - Mirror/36 Hrs	1.007 Inches	16
16	Dist. Water	#1 - Mirror/39 Hrs	.504 Inches	16
17	Dist. Water	#1 - Mirror/45 Hrs	14,200 Btu/Hr - Ft^2	12
18	Dist. Water	#1 - Mirror/48 Hrs	.125 Inches	16
19	Dist. Water	#1 - Mirror/53 Hrs	9,800 Btu/Hr - Ft^2	11
20	Dist. Water	#1 - Mirror/57 Hrs	19,100 Btu/Hr - Ft^2	Thermocouple Failure
21	Dist. Water	#1 - Mirror/64 Hrs	19,200 Btu/Hr - Ft^2	13
22	Dist. Water	#1 - Mirror/69 Hrs	19,200 Btu/Hr - Ft^2	13
23	Ethyl-Alcohol	#1 - Mirror/77 Hrs	10,500 Btu/Hr - Ft^2	17/Same Surface as used in 10 - 22
24	Ethyl-Alcohol	#1 - Mirror/82 Hrs	8,300 Btu/Hr - Ft^2	17
25	Ethyl-Alcohol	#1 - Mirror/86 Hrs	10,200 Btu/Hr - Ft^2	17

SUMMARY OF EXPERIMENTAL RUNS (continued)

Run Number	Test Fluid	Surface/Condition	Constant Water Level/ Heat Flux	Results Shown in Figure No./Comments
26	Ethyl-Alcohol	#1 - Mirror/90 Hrs	6,600 Btu/Hr - Ft^2	17
27	Ethyl-Alcohol	#1 - Mirror/94 Hrs	12,800 Btu/Hr - Ft^2	17
28	Dist. Water	#2 - Mirror/Polished	14,500 Btu/Hr - Ft^2	14/Lip Damaged in assembling
29	Dist. Water	#2 - Mirror/21 Hrs	14,800 Btu/Hr - Ft^2	14
30	Dist. Water	#2 - Mirror/32 Hrs	14,600 Btu/Hr - Ft^2	14
31	Dist. Water	#2 - Mirror/44 Hrs	14,500 Btu/Hr - Ft^2	14
32	Dist. Water	#1 - Grooved/7 Hrs	14,500 Btu/Hr - Ft^2	19
33	Dist. Water	#1 - Grooved/13 Hrs	10,300 Btu/Hr - Ft^2	19
34	Dist. Water	#1 - Grooved/16 Hrs	20,200 Btu/Hr - Ft^2	19
35	Dist. Water	#1 - Grooved/22 Hrs	15,000 Btu/Hr - Ft^2	19
36	Dist. Water	#2 - Sintered/7 Hrs	14,900 Btu/Hr - Ft^2	20/Nickel Mesh Sintered to Surface
37	Dist. Water	#2 - Sintered/15 Hrs	14,800 Btu/Hr - Ft^2	20

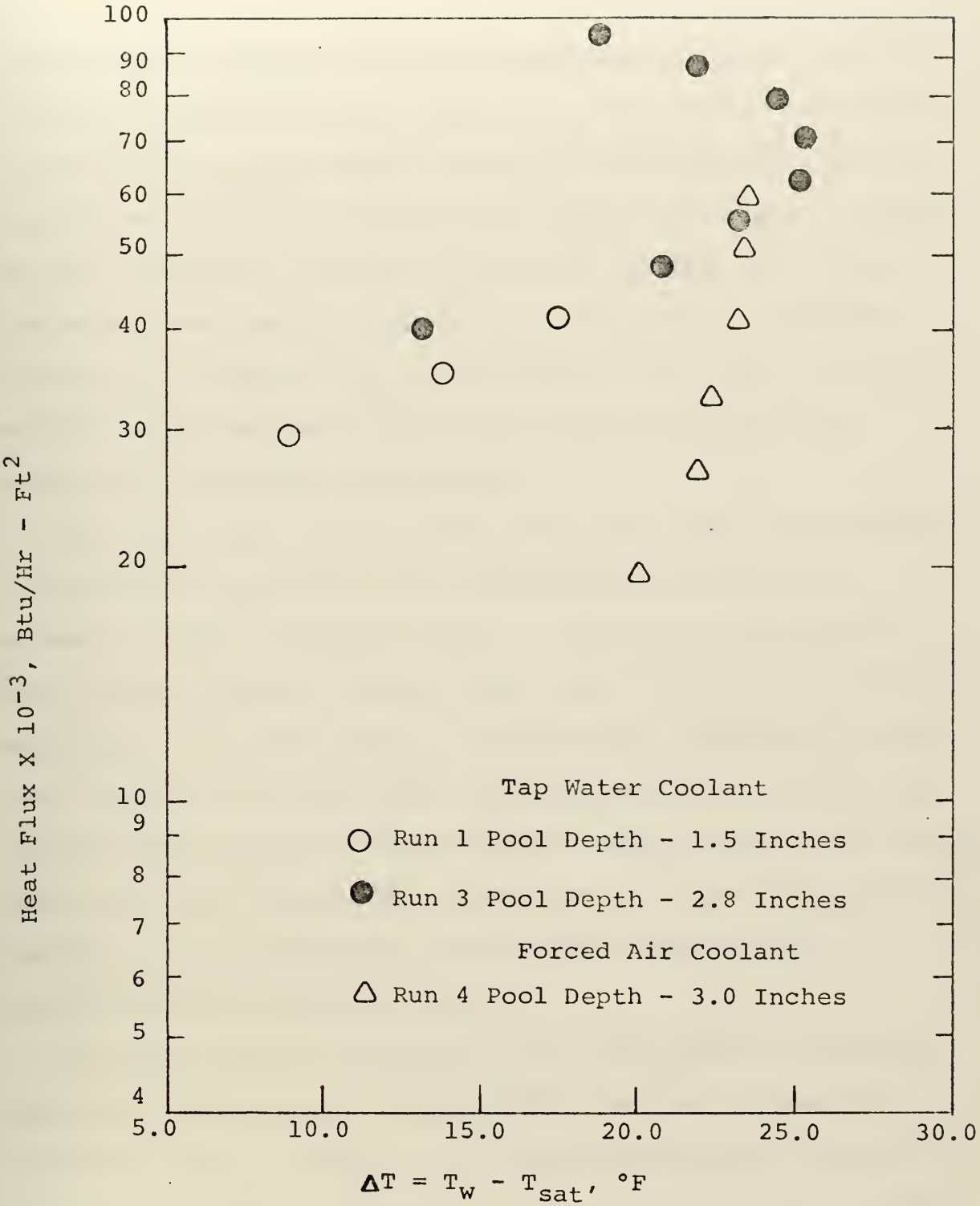

Figure 4. Testing of Experimental Apparatus. Effect of Forced Coolants

utilizing an enclosed heat exchanger-pumping system capable of maintaining the coolant water at a few degrees less than the saturation temperature; however, this equipment was not readily available and an alternate method was tried. Results of Run 4 (Figure 4) showed an improved boiling curve when forced air was used as a coolant; nevertheless, a decision was made to eliminate all forced coolant and leave the glass exposed to the ambient temperature which appeared to be sufficient to condense the vapors.

The heat flux computed from the power input was compared to the heat flux based on the temperature profile in the nickel cylinder for Runs 4 and 5. The results indicated a heat loss of 13% and 19% for these runs respectively. The majority of the heat loss was through the insulation and thus was a function of the manner used in packing the insulating material which varied every time the apparatus was taken apart. Because of this substantial power loss, the heat flux calculated from the temperature gradient was the one used in correlating all subsequent data.

The heat transfer apparatus and experimental techniques were then evaluated by obtaining data on pool boiling of distilled water. Figure 5 shows pool boiling data for Run 5 at .995" compared to Rohsenow's correlation for pool boiling with a surface-fluid combination of water-nickel (C_{sf} = .006) [14]; to the pool boiling data of Kunz, et al. [12] from an Inconel flat plate; to the pool boiling data from a square stainless steel surface of Alleavitch[5]; and to the pool

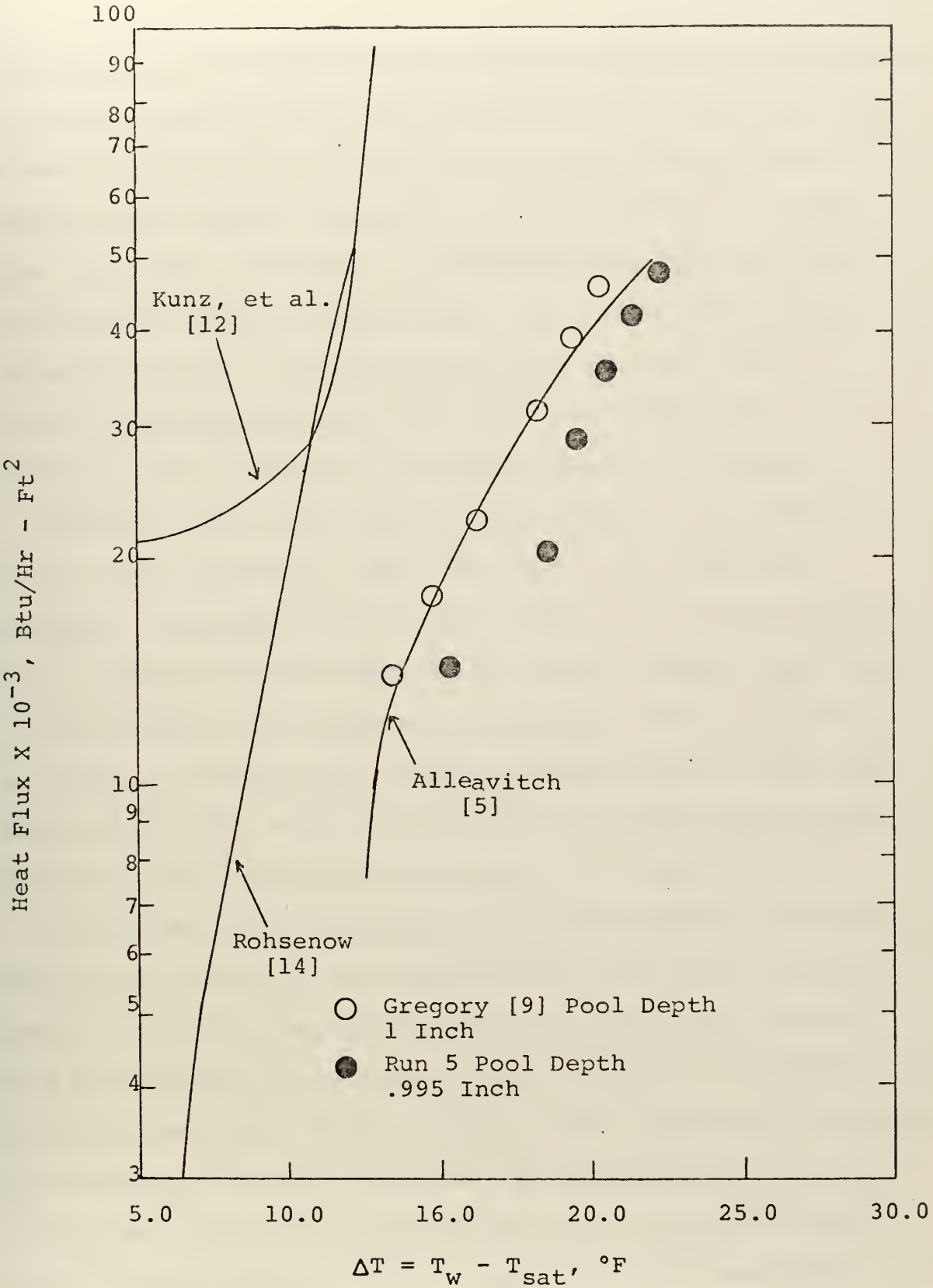

Figure 5. Comparison of Pool Boiling Results.

boiling data of Gregory [9] utilizing a similar test apparatus. The displacement of the data from Rohsenow's correlation was assumed to be due to the difference in the nature of the working fluid-surface interface. The displacement of the data from those of Gregory is believed to be caused by the difference in surface preparation. Gregory's surface was roughened with No. 240 Three-M-Ite Elek-Tro-Art cloth to promote nucleate boiling, while the metal surface for this study had been polished on a diamond wheel to 1 micron.

Figure 6 shows the effect of pool depth on the boiling curve. Pool depths of .995, .495, and .255 inches were compared. The curve shift to the right at .255 inches indicates a substantial decrease in the heat transfer coefficient at this liquid level; however, the cause of this shift was not known. Rohsenow [14] suggests that an aging effect may exist even though care was taken in repolishing the surface using the same repolishing technique as in Runs 5 and 6.

As the heat flux increased it was impossible to keep the water level constant, so another method was tried in which a constant heat flux was applied and the water level varied. This was similar to the methods used by Patten and Turmeau [11] and Nishikawa et al. [10]. Runs 8 and 9 were used to evaluate this method at two heat fluxes. It was noted that the A. C. input power fluctuated randomly and a D.C. regulated power supply was acquired in order to stabilize the power input for future runs.

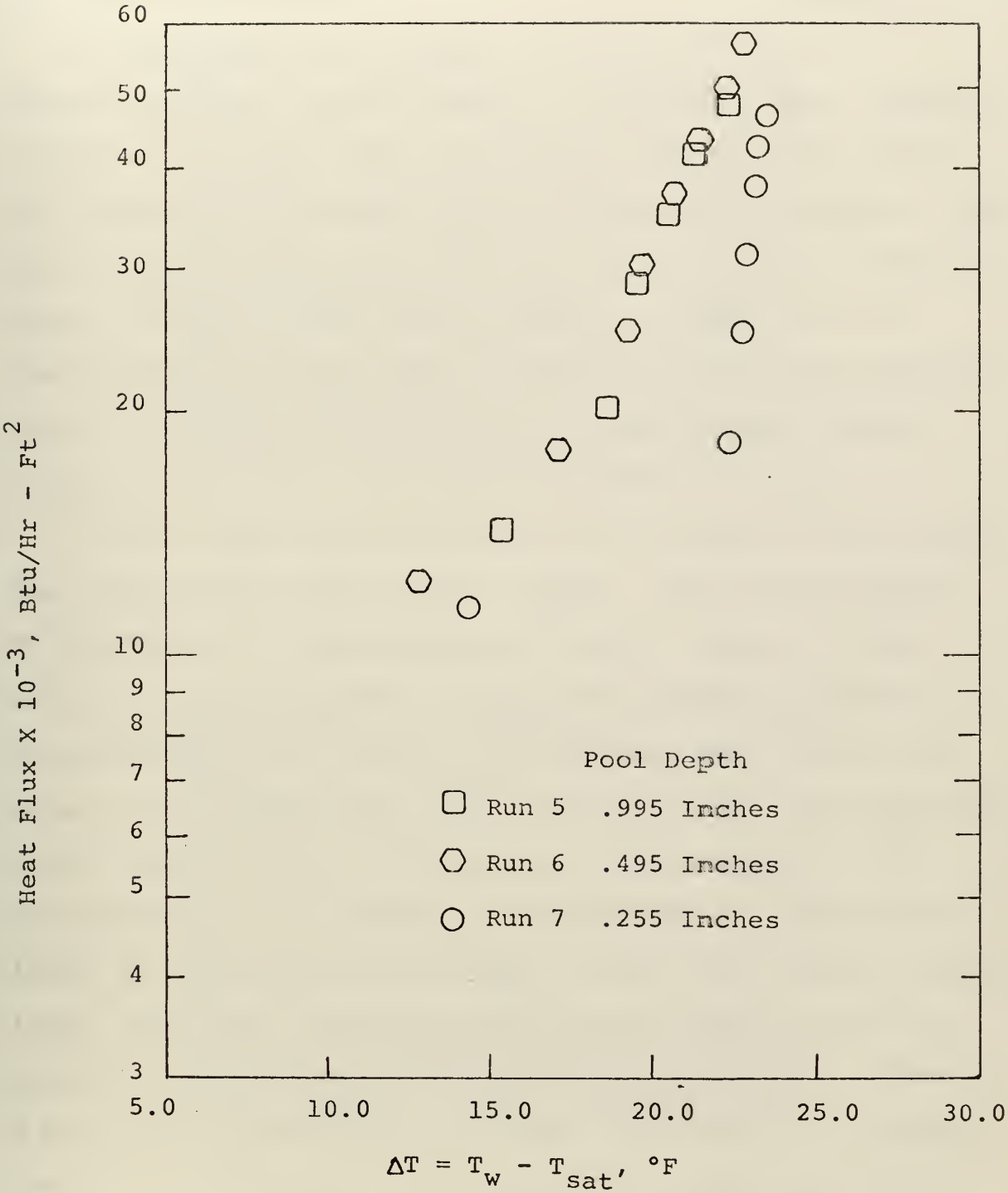

Figure 6. Testing of Experimental Apparatus. Effect of Pool Depth

B. ASPECT OF BOILING

During normal pool boiling, water circulates in a specific pattern; flowing upward in the center area, downward along the container walls and finally flowing inward toward the center of the heating surface to repeat the process. This type of pattern was found to occur in levels above 1 inch as shown in Figure 7 for a water level of 2 inches, and is characterized by the pyramid form the flow of bubbles project. Below 1 inch this specific pattern ceases and the bubbles climb straight up to the surface, as shown in Figure 8.

In the liquid range from 1.0" to 0.2 inches, it was noted that vapor domes formed on the liquid. These domes formed as the result of the coalescing of small bubbles as they leave the boiling surface. Vapor dome formation appeared to be influenced by two factors, the liquid level and the heat flux. At a constant heat flux the size of the dome increased as the liquid level was decreased. This increase in dome size appears to be a result of the decrease in liquid circulation as the level was decreased. While at a constant liquid level, dome size increased with increasing heat fluxes as a result of the increased number of nucleating sites. Figures 9 and 10 are photographs of a vapor dome forming at a liquid level of 1/2 inch and a heat flux of approximately 15,000 Btu/Hr - Ft^2. These domes are 1 1/4 - 1 1/2 inches in diameter. In several cases, one vapor dome would cover the entire heating surface. These extremely large domes were noted at heat

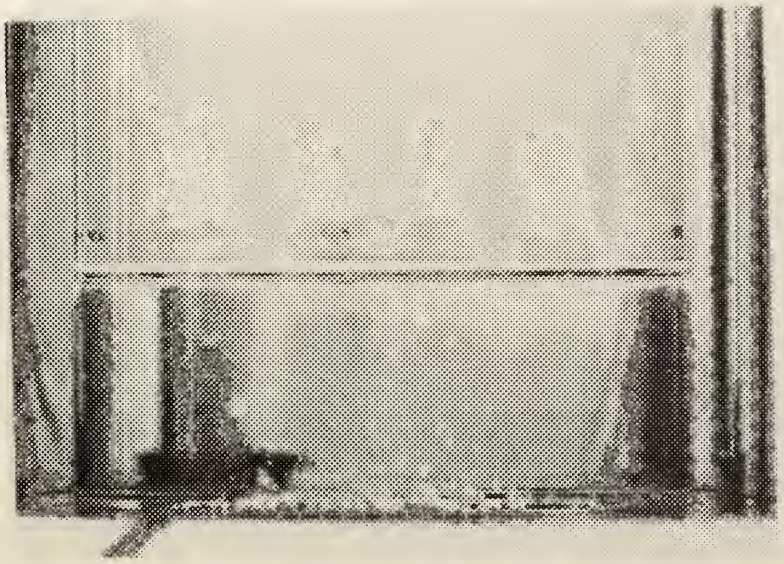

Figure 7. Pool Boiling - Depth 2 Inches

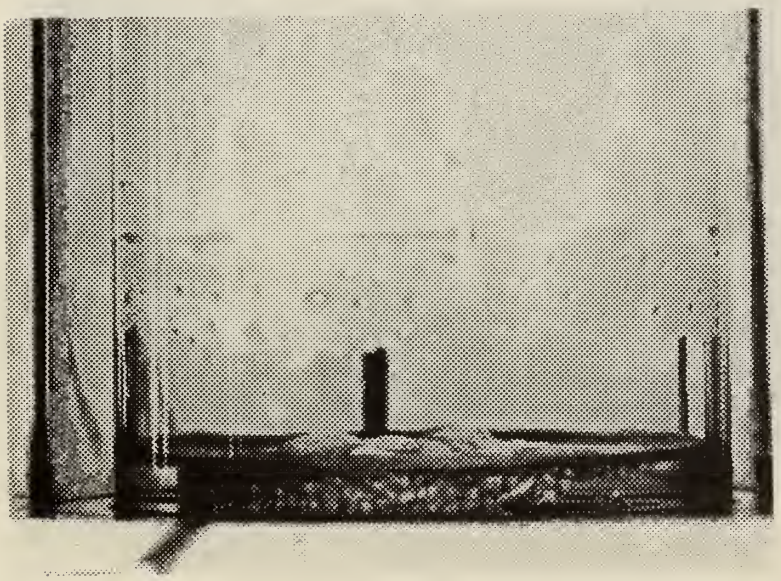

Figure 8. Pool Boiling - Depth 1/2 Inch

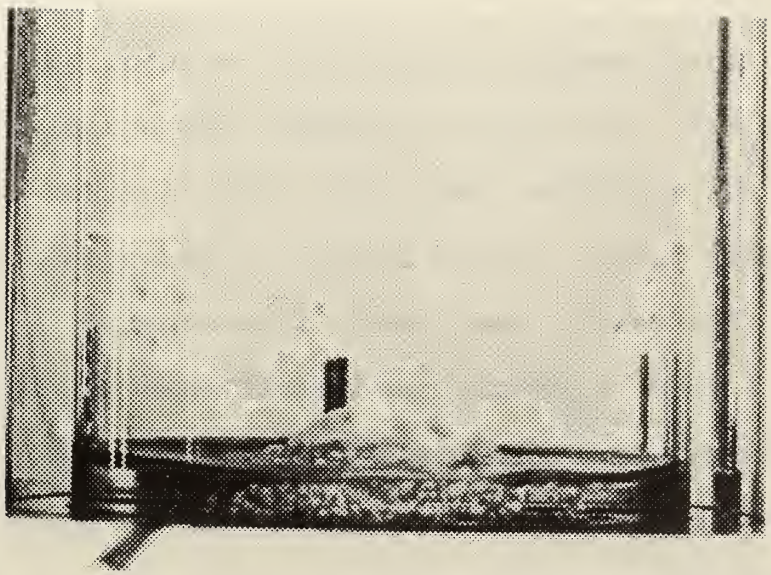

Figure 9. Vapor Dome Formation

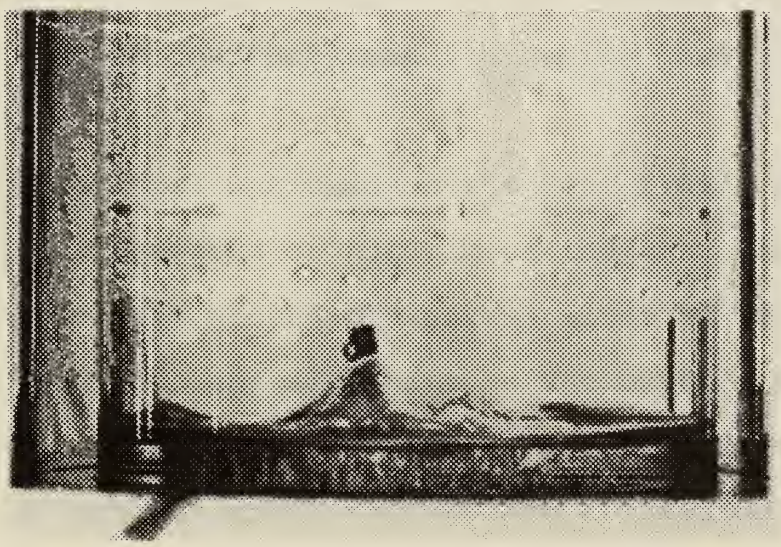

Figure 10. Vapor Dome Formation

fluxes of 18,000 - 25,000 Btu/Hr - Ft^2 and at liquid levels between .2 - .4 inches. Stability of these domes decreased as heat flux increased; however, in the .6 - .2 inch liquid level with a constant heat flux, the stability remained constant with decrease of liquid level. Domes remained in tact for 10 - 15 seconds at lower heat fluxes and 1 - 2 seconds at higher heat fluxes used in this study.

Since bubbles form from nucleating sites, an attempt was made to investigate the effect of heat flux and liquid level on the number of nucleating sites. It was quite evident from the runs at a constant liquid level that as heat flux is increased, the number of active nucleating sites increased. This increase in nucleating sites was not evident however under conditions of constant heat flux while lowering the liquid level.

When ethyl-alcohol was used on the test fluid, rogue nucleating sites appeared on the rim of the test surface and formed a 360° curtain around the active sites on the surface, thus interfering with any flow pattern the bubbles might have formed. It was noted that the bubbles released from rogue sites climbed straight up to the surface at liquid levels below 1 inch. Levels above 1 inch were not checked.

With ethyl-alcohol no large vapor domes formed. In fact, domes larger than 1/4 inch were rare. The population of domes was much greater than with distilled water because of the coalescing of bubbles in water. Individual bubble diameters

appeared to be approximately 1/3 the size of bubbles formed in distilled water. The increase in nucleating sites and bubble population as a result of an increase in heat flux was much more evident than in distilled water.

C. REPRODUCIBILITY AND AGING

The time required to disassemble the boiling apparatus, remove the test surface and refinish it in order to reproduce results, was approximately 8 hours. This time, although well spent, was considered excessive and another method for reproducing results was desired. Rohsenow [14] points out that experience teaches that aged surfaces have higher required ΔT for a given heat flux. Initial runs carried out in this study under similar conditions indicated the presence of this aging effect on the test surface as shown in Figure 11. It should be noted that during these aging runs no attempt was made to clean or refinish the test surface and that distilled water was used as the test fluid. This aging effect may be caused by a scale or deposit formation from the boiling liquid, or as a result of oxidation or other chemical reactions. When this happens the nucleating site(s) may shrink requiring higher superheat for activation.

Additional runs were conducted to determine if this aging effect could be minimized after several hours of boiling. Results shown in Figures 12 and 13 indicate that the aging effect diminishes with boiling time. These results also

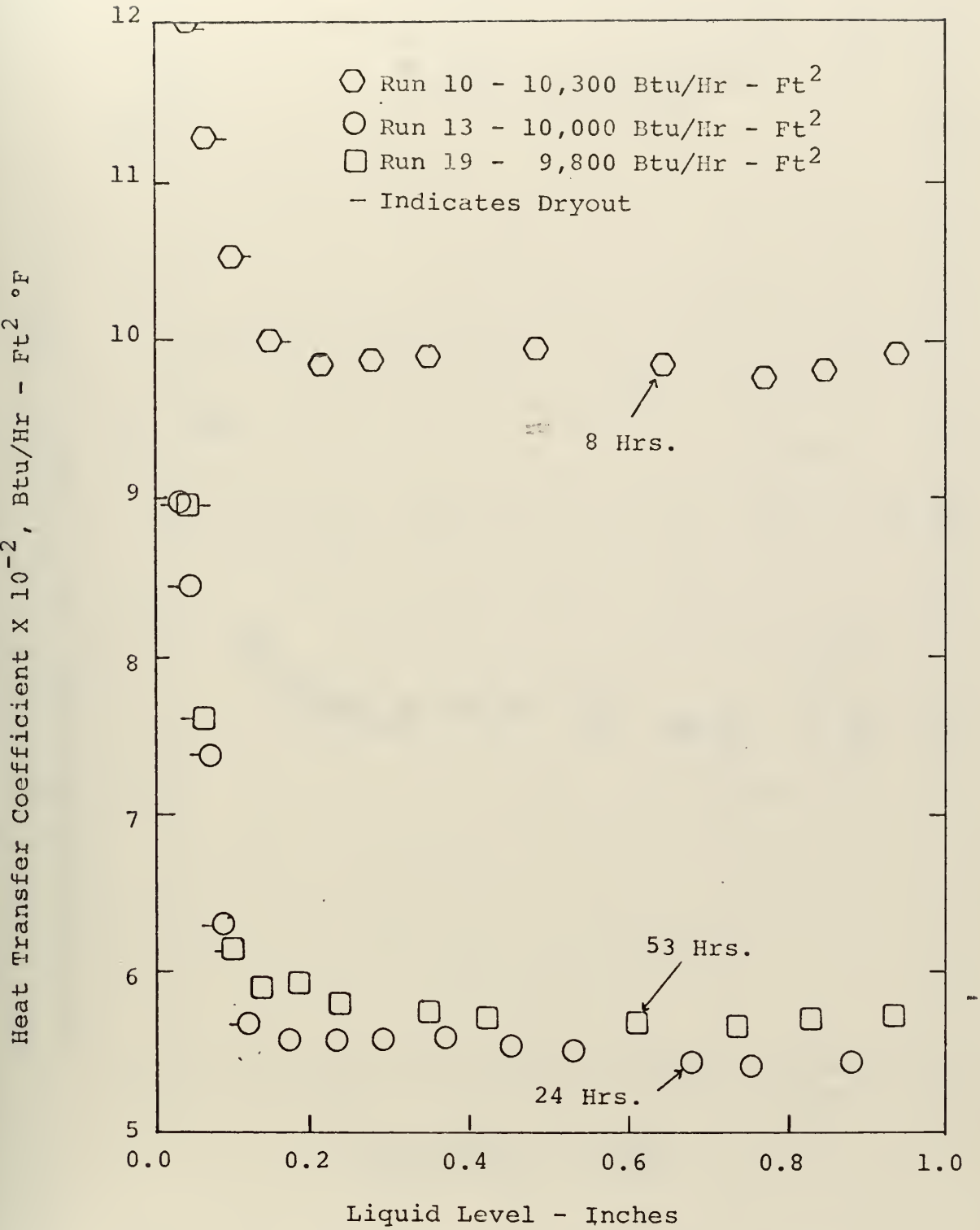

Figure 11. Effect of Aging on Boiling Surface #1 @ 10,000 Btu/Hr - Ft^2

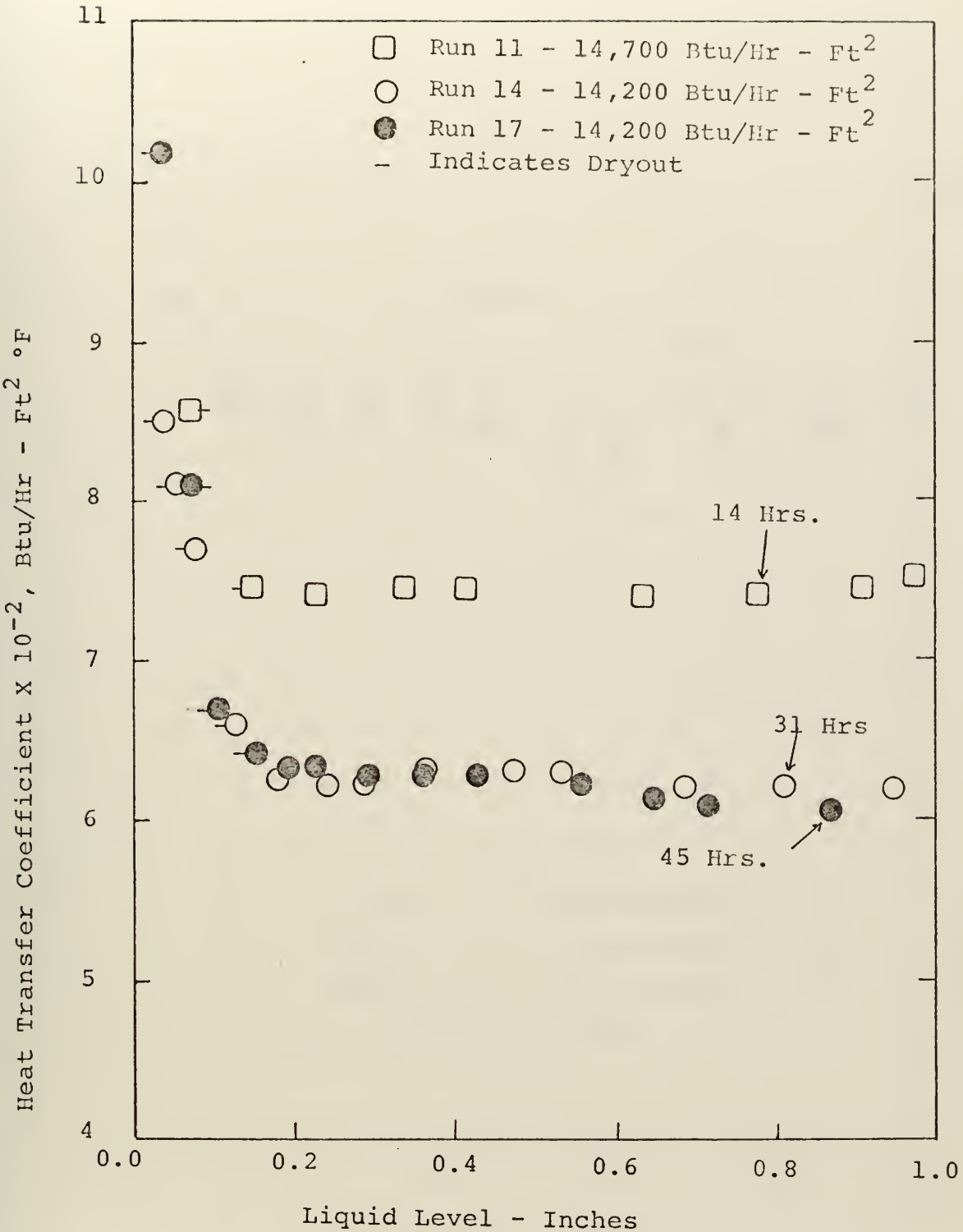

Figure 12. Effect of Aging on Boiling Surface #1 @ 14,000 Btu/Hr - Ft^2

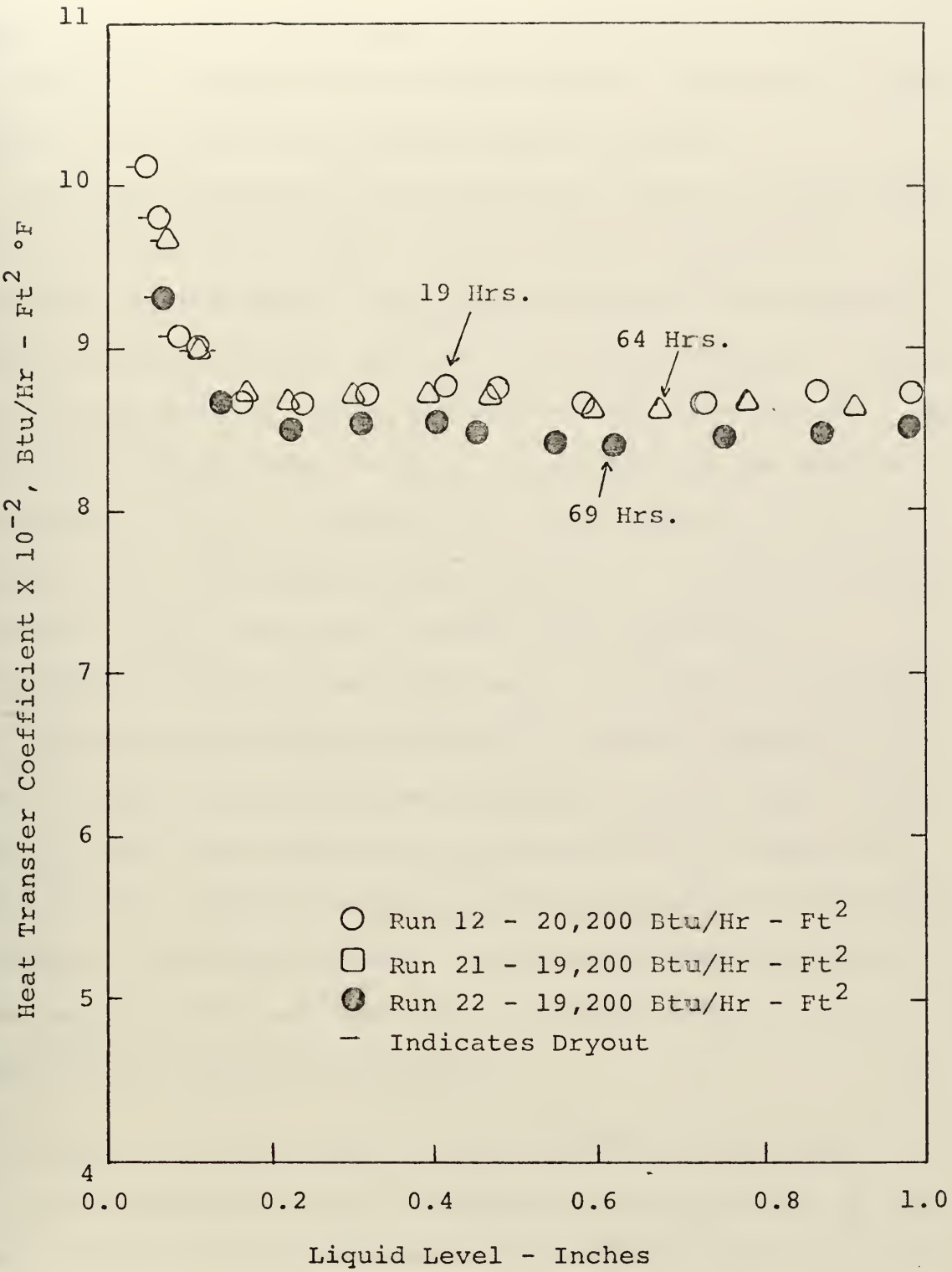

Figure 13. Effect of Aging on Boiling Surface #1 @ 19,000 Btu/Hr - Ft^2

indicate that when the aging effect subsides at one heat flux, it appears to subside at all heat fluxes. Higher heat fluxes appear to age the surface much faster, however.

Thus reproducibility of results was found to be possible once the surface had aged. Reproducibility between two surfaces was attempted. Two nickel surfaces were machined similarly and polished utilizing the same technique. Results of tests on surface 1 were discussed above, and surface 2 was tested to verify these results. In assembling the boiling apparatus the rim of surface No. 2 was accidently bent resulting in a dish-shaped surface profile. The appearance of cracks at the rim/surface interface may have acted as additional nucleate sites which were not present on surface #1; therefore, no attempt was made to compare results to see if reproducibility between surfaces was possible. However, 4 runs were conducted on this surface to verify the aging effect noted on surface #1 and the ability to reproduce results on the same surface. As shown in Figure 14, the same aging effect and ability to reproduce results on the same surface occurred on surface 2.

D. EFFECT OF LIQUID LEVEL ON HEAT TRANSFER COEFFICIENT

An investigation into the effect of liquid level on the heat transfer coefficient was conducted along with the study of reproducibility and aging. Results are shown in Figure 15, which is a graph of the heat transfer coefficient (h, Btu/Hr - Ft^2 - °F) vs. liquid level (inches) during runs at 3 constant heat fluxes on a surface where the aging effect has subsided.

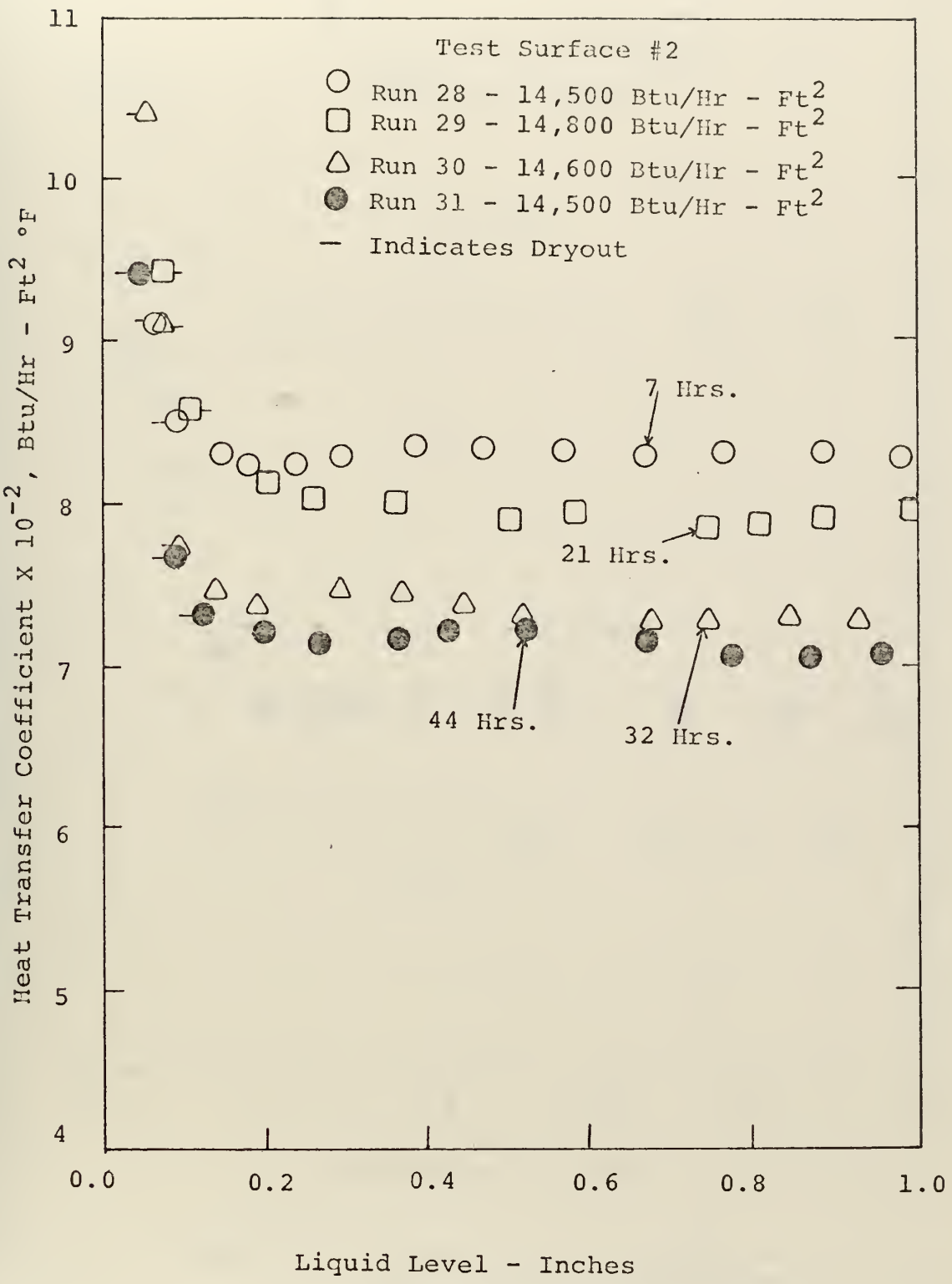

Figure 14. Effect of Aging on Boiling Surface #2.

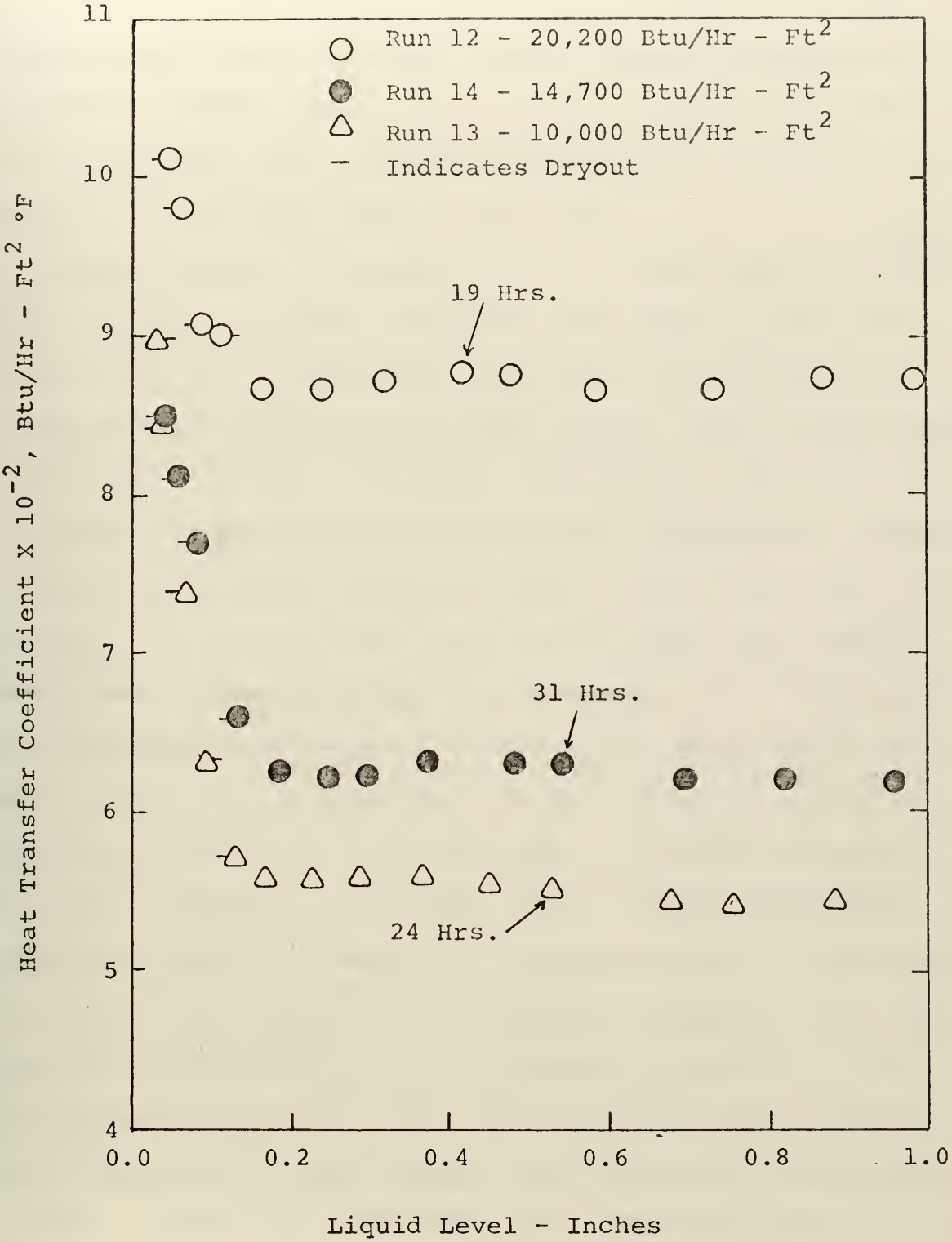

Figure 15. Effect of Liquid Level on Heat Transfer Coefficient.

In actuality, the constant heat flux was assumed to be the average heat flux, determined from the temperature profile, encountered during a run, which resulted in an uncertainty of $\pm$ 400 Btu/Hr - Ft^2. Liquid levels between 1 inch and 0.040 of an inch were used in this study.

Liquid levels in the range 0.2 - 1.0 inch appear to have little effect on the heat transfer coefficient at the heat fluxes studied. In this level range the heat transfer coefficient would vary about the same average value, approximately $\pm$ 15 Btu/Hr - Ft^2 °F. Of course, as expected, the higher the heat flux, the greater the heat transfer coefficient. One of the interesting points noted in Figure 15, and also noted in Figures 11, 12, and 13, was the fact that the heat transfer coefficient decreased slightly in the range 1.0 - 0.75 inches; then increased slightly to a maximum in the 0.4 - 0.75 inch range; followed by a decrease to a new low heat transfer coefficient in the 0.2 - 0.4 inch range. As noted in Run 31, as shown in Figure 14, the above heat transfer coefficient results occurred on a second test surface under an identical situation. This appears to be in partial agreement with the results of Nishikawa, et al. [10] except in the 0.4 - 0.75 inch liquid level, where they had the heat transfer coefficient decreasing by slow degrees with decreasing liquid level in the 1.2 inch - 0.4 inch range. No firm conclusions can be drawn here until additional research is completed.

Levels below 0.2 appear to have a tremendous effect upon the heat transfer coefficient as shown in Figure 15. An abrupt increase in the coefficient was noted, in most cases,

below the 0.2 inch liquid level. In each case where this increase was noted, dryout occurred on the test surface. Dryout was characterized by a sudden fluctuation in the thermocouple temperatures, and by a bright spot appearing on the surface. In this range of liquid levels the lower the heat flux the more remarkably the liquid level affects the heat transfer coefficient. It should be noted here, that in Figure 15 it appears that dryout initially occurred at the same liquid level for all heat fluxes. This is strictly a coincidence because no attempt was made to find the exact level where dryout commences and the uncertainty in the liquid level at a heat flux of 20,000 Btu/Hr - Ft^2 was $\pm$ .015 inch.

Figure 16 shows the effect of pool boiling at liquid levels of 1 inch, 1/2 inch and 1/8 inch. The pool boiling curve at 1/8 inch shows an abrupt shift to the left indicating a much higher heat transfer coefficient. This coincides with the results of Gregory [9] and Nishikawa, et al. [10].

The effect of liquid level on the heat transfer coefficient was also investigated with ethyl-alcohol as the test fluid. Five runs were conducted at various constant heat fluxes with the results shown in Figure 17. The results were similar to those described above with distilled water but with much lower values of heat transfer coefficient, as expected. The effect of liquid levels in the 1.0 - 0.4 inch range appears to be rather small. No increase in heat transfer coefficient

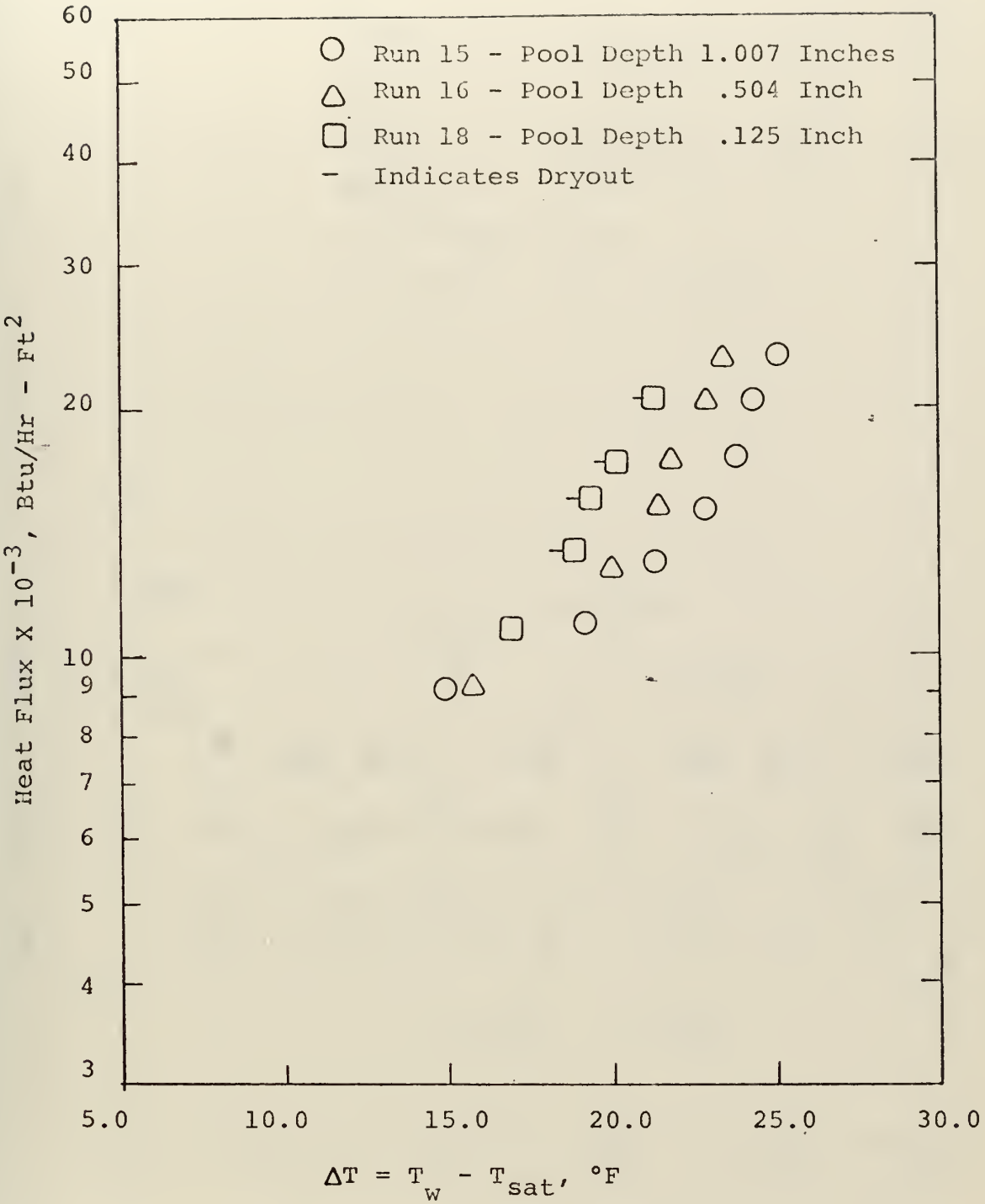

Figure 16. Effect of Pool Depth

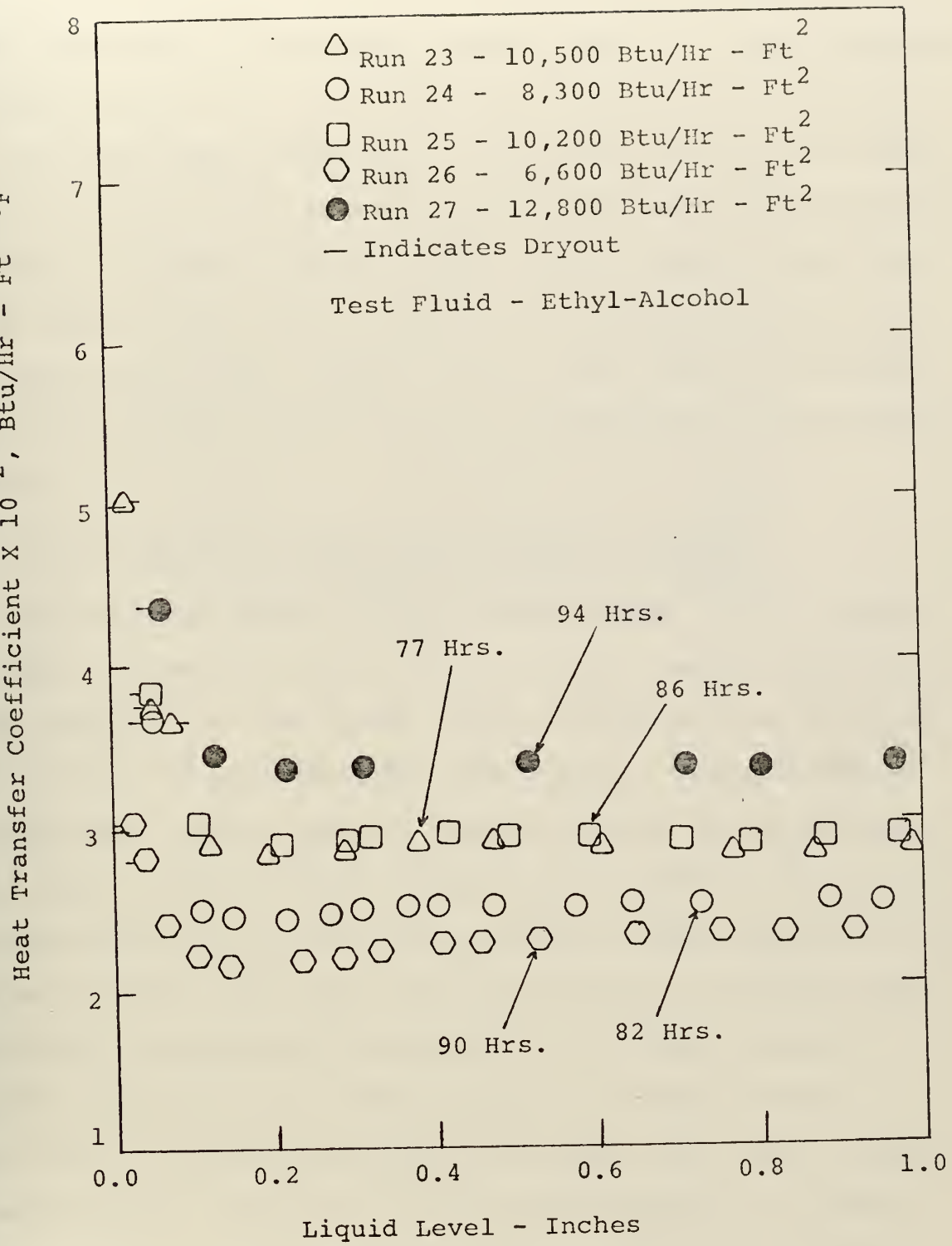

Figure 17. Effect of Liquid Level on Heat Transfer Coefficient Using Ethyl-Alcohol

was noted in this 0.4 - 1.0 inch liquid level. This concurs with the results of Nishikawa, et al. [10]. A slight decrease occurred in the 0.4 - 0.2 inch range with an abrupt increase in the coefficient occurring in the 0.080 - 0.120 inch range. This increase in heat transfer coefficient was accompanied by dryout of the test surface in most cases; however, this was much harder to see than in the distilled water case because no large vapor domes formed, and the large number of nucleating sites present prevented good visualization of the boiling surface.

E. VAPORIZATION OF LIQUID LEVELS BELOW 0.2 INCH

As mentioned before, liquid levels below 0.2 inch appear to have a tremendous effect upon the heat transfer coefficient. With water as the test fluid, dryout coincided with an abrupt increase in the heat transfer coefficient. Dryout occurred in two ways: dryout under a dome and dryout in the absence of a dome. The first way, dryout under a dome, is the result of internal pressure developing within the dome forcing fluid below the dome aside until the test surface is exposed under the dome. In addition the presence of the dome prevented bubble microconvection effects across the test surface. This type of dryout was present throughout the liquid levels studied below .200 inch. It was characterized by a sudden fluctuation in the thermocouple temperatures, and a bright spot appearing under the dome. At levels above 0.060 inch, even with this type of dryout occurring, it was possible to sustain nucleate boiling. Figure 18 shows vapor domes

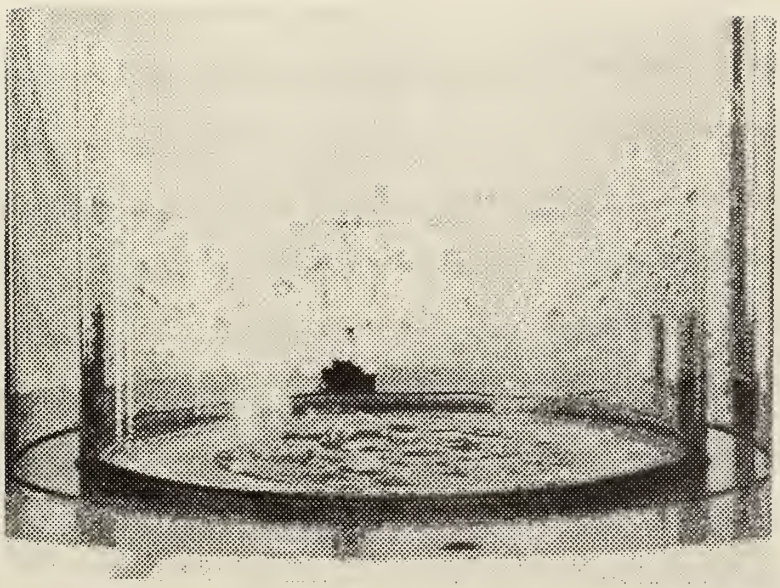

Figure 18. Dome Formation at Liquid Level .090 Inch

forming at 0.090 inch of water, with dryout occurring under some domes.

Below 0.060 inch, the second type of dryout, dryout without a dome, would occur along with dryout under a vapor dome. This type of dryout was characterized by a much higher drop in surface temperature along with a faster spreading rate. This spreading could be controlled for a while in the range of 0.040 - 0.060 inches by means of the vapor domes pushing fluid over the exposed surface; however, around 0.040 inch dryout without a dome becomes the prevalent form and would spread across the test surface, eventually causing an overheating of the test surface.

These results were similar to those of Patten and Turmeau [11], with the exception that they found vapor domes ceasing to appear on the surface below the 0.080 water level. In all levels during this study, vapor domes continued to appear until forced aside by the spreading dryout without a dome. Although this study only went down to liquid levels of 0.040 inch, while Patten and Turmeau went as low as 0.020, no specific range was found below which just dryout without a dome was present.

What causes this increase in the heat transfer coefficient as liquid level decreases is still not known. Pure conduction could cause a substantial increase in very small liquid levels ($\simeq$ .005 inch); however, by the time this could happen entire dryout of the surface would most likely occur. As the liquid level is lowered the intense bubble-produced agitation of the

liquid layer decreases, and results in a lower heat transfer coefficient. Johnson, Jansen and Owzarski [15] suggest that the Marangoni effect may be the additional mechanism which, when combined with a bubble-produced agitation mechanism, may result in this increased heat transfer coefficient. Basically, the Marangoni effect postulates very rapid surface renewal and internal circulation as the result of lateral gradients in surface tension of the film surrounding a bubble; therefore, as dry spots form under a dome, surface tension effects cause large velocities to exist. Additional investigation is necessary utilizing visual recording techniques before any conclusions can be drawn as to the causes of this increase in heat transfer coefficient.

When ethyl-alcohol was used as the test fluid, it was hard to see if dryout occurred under domes because of their small size and number present. In the range 0.080 - 0.120 inches when temperatures fluctuated and the heat transfer coefficient increased, small domes along the edge of the test surface were observed pushing fluid aside and expanding down to the surface itself. This same type of dome formation was assumed to be happening over the entire test surface, as no visual signs of dryout under a dome were noticed when looking down from the top, as in the case of distilled water. Dryout without a dome appeared in the 0.040 - 0.060 inch level; however, even with this form of dryout present nucleate boiling could be maintained as a result of the wettability of ethyl-alcohol. Below 0.040 inch, vapor domes ceased to exist and dryout of the entire surface gradually occurred.

F. SPECIAL SURFACES TO IMPROVE THE HEAT TRANSFER COEFFICIENT

1. Grooved Surface

A grooved surface, utilizing distilled water as the test fluid, was studied to determine its effect on the heat transfer coefficient. Results of this study are shown in Figure 19. An aging effect was immediately noticed between Run 32 and 35. With the exception of Run 32, the effect of the grooved surface on the heat transfer coefficient was similar to that observed during tests on a mirrorlike surface with distilled water (Runs 10 - 22). Run 32, the first run on the new surface, has a similar profile to that suggested by Nishikawa, et al. [10] for a smooth surface.

The numerical values of the heat transfer coefficient are similar to those observed earlier on a mirrorlike surface in the 0.2 - 1.0 inch liquid level. Below 0.2 inch the grooved surface shows an abrupt increase in the heat transfer coefficient, which is similar to the mirrorlike surface; however, this increase occurs without dryout. Without the grooves, dryout under a dome occurred in the 0.060 - 0.200 inch range followed by a combination of dryout in absence of a dome and dryout with a dome in the 0.040 - 0.060 inch range. With grooves, no dryout was observed until below the 0.030 inch level. The observed type of dryout was dryout in absence of a dome. Even with this type of dryout occurring it was possible to sustain nucleate boiling down to 0.015 inch. When dryout

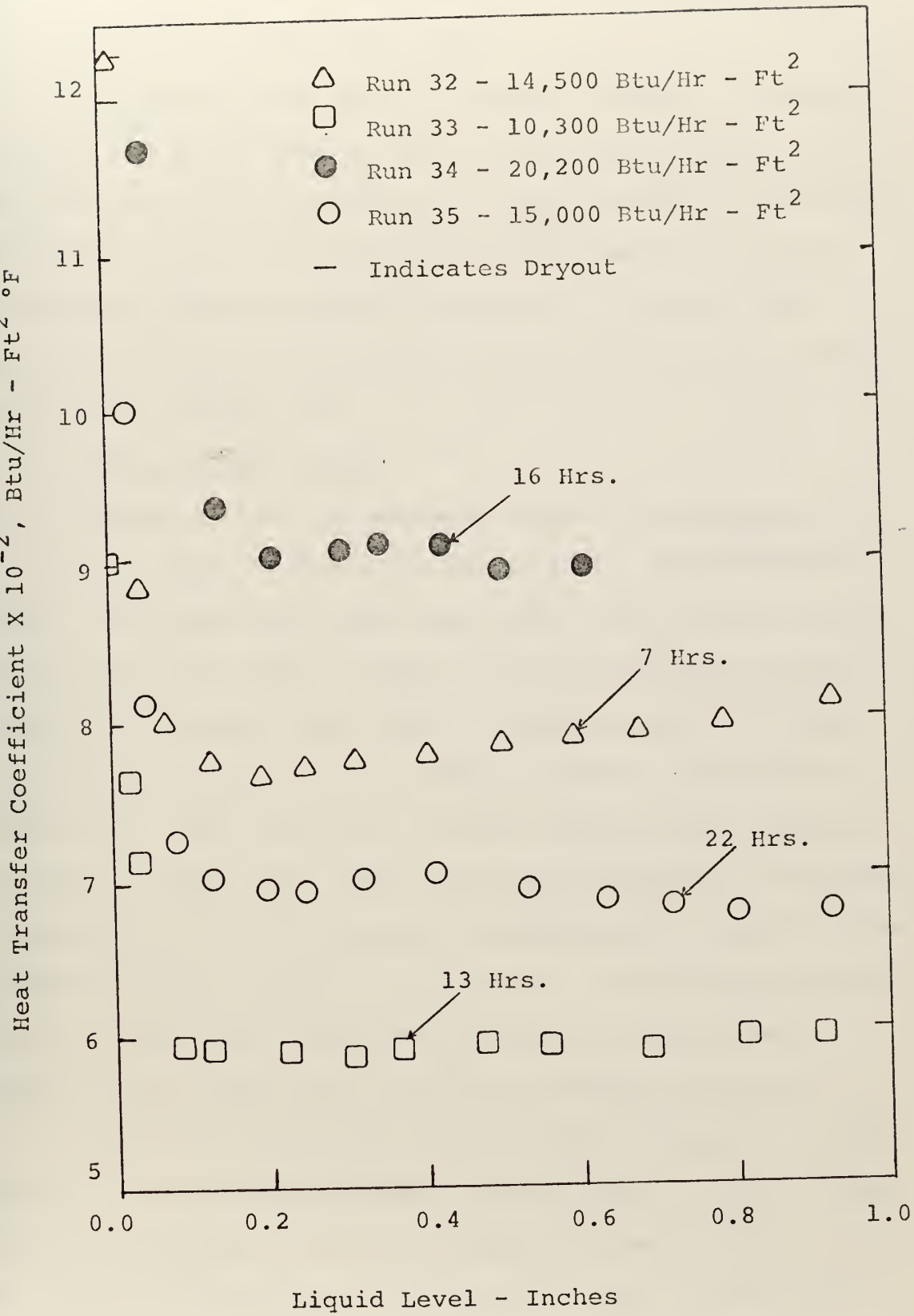

Figure 19. Effect of a Grooved Surface on Heat Transfer Coefficient

occurred on the surface, water would be transferred along the grooves to cover this dry spot.

It appears that grooves provide a means of obtaining a stable high heat transfer rate at low liquid levels. No study was made as to the effect of liquid level on the number of nucleate sites or the effect of heat flux on the sites. No analytical solutions were carried out to relate this higher heat transfer coefficient to the size of the grooves, shape of the grooves, etc.

2. Mesh Covered Surface

A mesh covered surface was studied to determine its effect on the heat transfer coefficient at various liquid levels. An attempt was being made here, to simulate a heat pipe to find out how the wicking material effected the heat transfer coefficient. The mesh, 4 layers of 40 x 50 nickel screen, was sintered onto the test surface as explained in Section III. The results of the two tests on this surface are shown in Figure 20. The appearance of the data indicates an increase on the heat transfer coefficient for depths above .2 inch in going from Run 36 to Run 37. This trend contradicts the aging data obtained previously on other test surfaces and is believed to be due to another mechanism.

Run 36 was characterized by bubbles streaming forth between the screen layers from 7 areas along the lip circumference, followed by a stream of bubbles from the center of the surface once every 20 - 30 seconds. When these center bubbles appeared a substantial drop in the thermocouple temperature was noted, followed by an increase in temperature

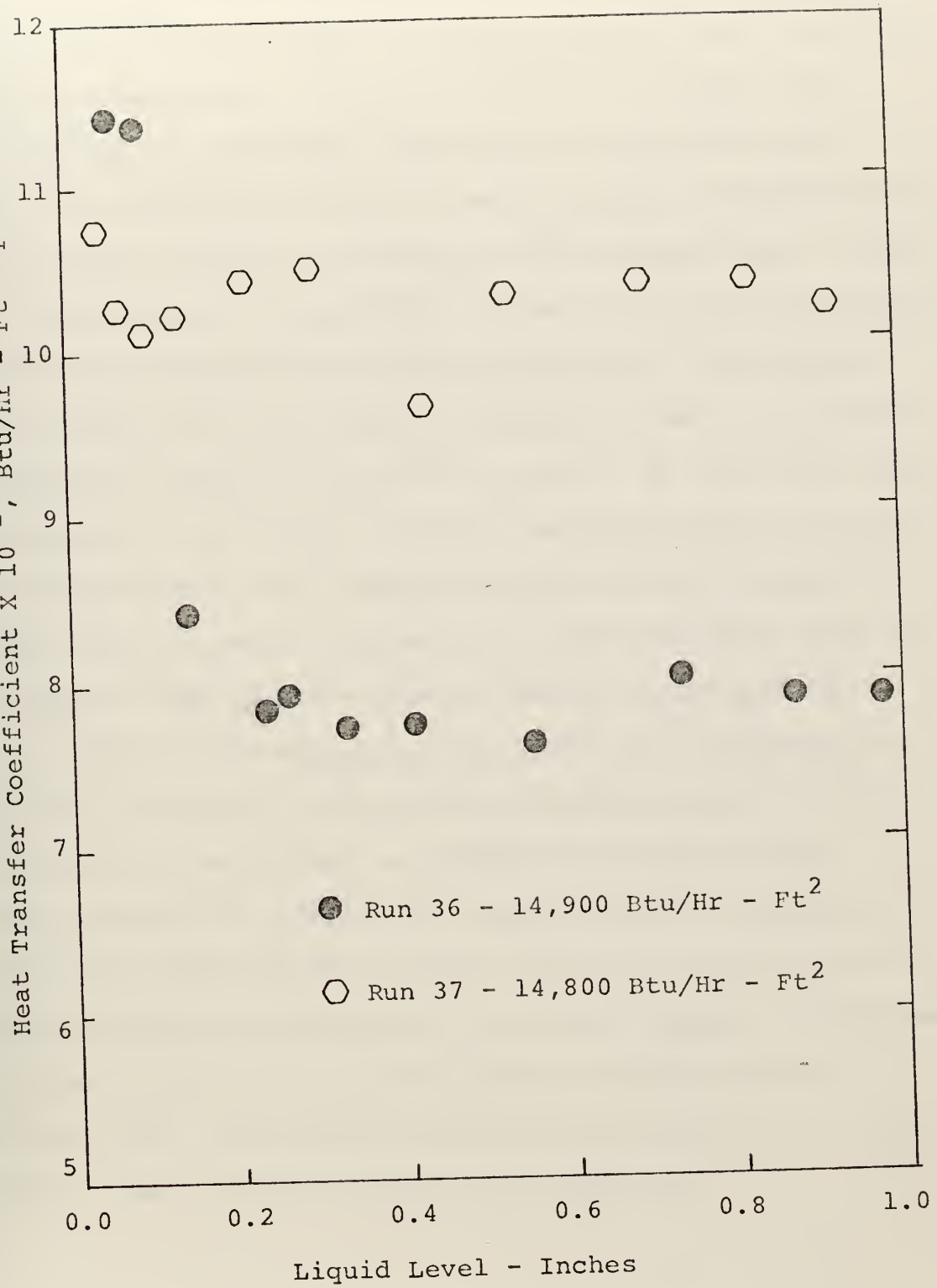

Figure 20. Effect of Sintered Screen on Heat Transfer Coefficient

until the next stream of bubbles. On the other hand Run 37 was characterized by bubbles streaming forth from 9 areas on the lip circumference with center bubbles released every 2 - 3 minutes. Very minor temperature fluctuations were noted when these center bubbles were released. The difference in the characteristics of these two runs suggest that a large vapor pocket was forming within the mesh during Run 36 causing the surface temperature to rise substantially. The vapor pocket would then force its way through the mesh and release its bubbles allowing the surface to cool. On the other hand, the majority of the vapor in Run 37 escaped through the mesh and out the sides. The abrupt increase in heat transfer at liquid levels below 0.2 inches during Run 36 also suggests some type of vapor pocket causing dryout on the surface.

From the observations made above and the results in Figure 20, it appears that a substantial increase in the heat transfer coefficient is possible utilizing a mesh covered surface, if a means for vapor escape is provided. As with all other surfaces tested during the study, no substantial increase or decrease in the heat transfer coefficient was noted in the 0.2 - 1.0 inch liquid level during any particular run. No firm conclusions can be made until further studies on mesh covered surfaces are completed.

V. CONCLUSIONS

1. During nucleate pool boiling from a horizontal disk, liquid levels in the 0.2 - 1.0 inch range appear to have little effect on the heat transfer coefficient.
2. Below liquid levels of 0.2 inch a rapid increase in the heat transfer coefficient occurs with the lowering of the liquid level, which appears to be the result of dryout on the test surface.
3. Two types of dryout occur below liquid levels of 0.2 inch: dryout under a vapor dome and dryout in absence of a dome. Both types occurred with working fluids used in this study; however, dryout under a dome was not as evident in ethyl-alcohol.
4. With water as the working fluid, vapor domes are present in levels above 0.040 inch and domes as large as the boiling surface are possible depending on the combination of heat flux and water level.
5. Aging effect present on all new or repolished surfaces diminishes with boiling for several hours. Higher heat fluxes result in faster subsiding of the aging effect. Reproducibility of results is possible once surface has aged.
6. Grooved surfaces appear to provide a means of obtaining a stable high heat transfer rate at water levels down to 0.015 inch.

7. The scattering of data on a mesh covered surface indicates the presence of vapor pockets; however, if a means is provided for vapor escape a much improved performance may be possible.

VI. RECOMMENDATIONS FOR FURTHER STUDY

1. Investigate nucleate boiling in liquid levels below 0.2 inch utilizing high-speed photography to determine the mechanism(s) which causes an increase in the heat transfer coefficient below 0.2 inch.
2. Raise the test surface above its supports for a clearer visual display.
3. Redesign the boiling apparatus so that the liquid level can be monitored closer. This would require a larger fluid container to prevent the motion of the fluid during boiling from interfering with the liquid level measurement.
4. Provide a fluid coolant just below the saturation temperature to condense the working fluid's vapor.
5. Investigate the effect of various groove sizes, shapes, etc., on the heat transfer coefficient at low liquid levels. Study the mechanism(s) of heat transfer from grooved surfaces.
6. Investigate the effect of various size mesh material, their shape, thickness, no. of layers, and orientation on the heat transfer coefficient at low liquid levels.

APPENDIX A

THERMOCOUPLE CALIBRATION PROCEDURE

Six metallic-sheathed copper-constantan thermocouples were utilized to measure the temperature gradient in the nickel cylinder and ultimately, through the use of the least squares method, to determine the temperature at the boiling surface. The properties of these particular metals proved them to be most suitable for the temperature range studied. A total of 8 thermocouples were calibrated to take care of any potential thermocouple problems.

To insure accuracy in measurement, the thermocouples were calibrated at fixed reference points spanning the experimental temperature range. These fixed reference points as recommended by Roeser and Lanburger [16] included:

1) Triple point of ice -- 0.01°C (32.02°F)
2) Boiling point of water -- Dependent upon atmospheric pressure
3) Freezing point of pure tin -- 231.88°C (449.38°F)
4) Freezing point of pure lead -- 327.4°C (621.32°F)

All calibration voltages were measured with the reference junction in a distilled water-ice bath and read with a Hewlett-Packard Data Acquisition System Model 2010C containing a guarded data amplifier and an integrating digital voltmeter. This instrument gave a printed digital output with an accuracy of $\pm$ 0.5 microvolts.

To measure the triple point of ice an ice bath, consisting of finely crushed ice made from distilled water, was contained in a 16-ounce thermos bottle and saturated with distilled water. Three determinations of the voltages for each thermocouple were made and the results averaged and listed in Table 2.

To measure the boiling point of water, a stoppered 600 milliliter glass beaker, vented to the atmosphere and filled with 300 ml distilled water, was heated with a standard hot plate until rapid boiling occurred. The water was allowed to boil for 15 minutes to remove entrapped air. The thermocouples were then inserted individually through the stopper to a point three-fourths of an inch above the boiling water surface, and at this point a valid reading of the vapor temperature voltage was measured. Three readings of voltages at this particular pressure were made and the results averaged and listed in Table 2.

To calculate the equilibrium temperature of boiling water the atmospheric pressure was recorded from an aneroid barometer and the following equation used [16]:

$$T_{sat} = 100 + 28.012 \left(\frac{P}{P_o} - 1\right) - 11.64 \left(\frac{P}{P_o} - 1\right)^2 + 7.1 \left(\frac{P}{P_o} - 1\right)^3$$

where

T_{sat} = equilibrium (saturation) temperature in degrees C

P = local atmospheric pressure in mm Hg

P_o = standard atmospheric pressure in mm Hg

To measure the freezing point of tin, a National Bureau of Standards tin sample (melting point - 231.88°C) was heated in a stoppered test tube in a Hoskins Electric Furnace. The thermocouple was inserted through the stopper in a glass protective tube into the molten tin to a depth of approximately 1 1/2 inches. Powdered graphite was sprinkled on the molten tin to retard oxidation. Once the tin was thoroughly molten, the furnace was secured, and the test tube removed and placed in an asbestos lined container. The temperature of the molten tin in terms of thermal emf of the thermocouple was then monitored with the Data Acquisition System until the freezing point was reached and passed. The freezing point of tin was characterized by an almost constant voltage (read every second) for a period of approximately 2 minutes. As noted by Von Vlack [17] the temperature of tin dropped below the freezing point and returned to a constant temperature which was considered the freezing point. Once the freezing point was determined, the test tube was placed back in the furnace and heated for a second time and the same process was carried out for another temperature reading on the same thermocouple. Each thermocouple was read twice and the results averaged and listed in Table 2.

In a similar manner the freezing point of lead was measured using a National Bureau of Standards lead sample (melting point 327.4°C). However, with lead no constant voltage was observed for longer than 10 seconds, therefore a millivolt vs. time curve was plotted and the inflection

point found and an uncertainty assumed around this point. A second set of data verified this point and the point with its uncertainty listed in Table 2.

Using the voltages obtained for the four fixed reference points to solve for the four unknown constants (Appendix B), the following equation was used to determine a temperature-voltage relation for each thermocouple:

$$T = A + BM + CM^2 + DM^3$$

where

T = thermocouple temperature in degrees F

M = thermocouple voltage in millivolts - mv

TABLE 2

THERMOCOUPLE CALIBRATION RESULTS

Thermocouple	Millivolts Observed			
	Triple Point 32.0°F/0.00 mv	Steam Point 212.34°F/4.286 mv	Tin Freezing Point 449.38°F/11.012 mv	Lead Freezing Point 621.32°F/16.473 mv
20	.041 + .001	4.314 ± .002	11.997 ± .002	16.450 ± .010 mv
21	.043 ± .001	4.300 ± .002	10.953 ± .002	16.388 ± .010 mv
22	.044 ± .001	4.318 ± .002	10.994 ± .002	16.436 ± .010 mv
23	.048 ± .001	4.328 ± .002	11.014 ± .002	16.449 ± .010 mv
24	.051 ± .001	4.331 ± .002	11.015 ± .002	16.467 ± .005 mv
25	.055 ± .001	4.336 ± .002	11.020 ± .002	16.478 ± .005 mv
26	.057 ± .001	4.339 ± .002	11.023 ± .002	16.478 ± .010 mv
27	.061 ± .001	4.342 ± .002	11.027 ± .002	16.478 ± .010 mv

APPENDIX B

SAMPLE CALCULATIONS

1. Thermocouple Calibration (thermocouple #20)

Utilizing a Least Squares Polynomial Fitting Subroutine (LSQPL2) for an IBM 360 computer, coefficients for the power series:

$$T(X) = A + BX + CX^2 + DX^3$$

were determined from observed dependent and independent variables found during the calibration of the thermocouples. For thermocouple 20 the observed dependent and independent variables were respectively:

a) The fixed calibration temperatures in degrees F:

32.02
212.34
449.38
621.32

b) Millivolts from calibration process corresponding to the fixed calibration temperatures:

.041
4.314
10.999
16.450

With these variables the resultant power series for temperature (T) as a function of millivolts (X) for thermocouple 20 was:

$$T(X) = 30.12597 + 45.74406X - 0.88978X^2 + 0.01786X^3$$

Similar solutions were obtained for the other thermocouples.

2. Data Reduction Program

With the aid of a data reduction program written for the IBM 360 the following values were determined:

T_{sat} - equilibrium (saturation) temperature, °F

T_w - surface temperature, °F

$T_w - T_{sat}$ - surface-saturation temperature difference, °F

k - conductivity, Btu/Hr - Ft - °F

$(Q/A)_P$ - heat flux from power input, Btu/Hr - Ft^2

$(Q/A)_T$ - heat flux from temperature profile, Btu/Hr - Ft^2

a) T_{sat} was determined from the equation:

$$T_{sat} = 100 + 28.012\left(\frac{P}{P_o} - 1\right) - 11.64\left(\frac{P}{P_o} - 1\right)^2 + 7.1\left(\frac{P}{P_o} - 1\right)^3$$

ex. Run 16 where P = 761.90 mm Hg

$$T_{sat} = 100 + 28.012\left(\frac{761.90}{760.00} - 1\right) - 11.64\left(\frac{761.90}{760.00} - 1\right)^2 + 7.1\left(\frac{761.90}{760.00} - 1\right)^3$$

T_{sat} = 100.07°C (212.12°F)

b) T_w was determined by utilization of the method of least squares for solving the equation:

$T_w = AX + B$ (see Appendix D)

ex. Run 16 - Data Point 3

With the necessary information from smooth data, the following sums were formed:

T_i
262.16
251.46
238.99
$\Sigma T_i = 752.61$

X_i
0.220
0.715
1.215
$\Sigma X_i = 2.150$

$T_i X_i$
57.68
179.79
290.37
$\Sigma T_i X_i = 527.84$

X_i^2
.048
.511
1.476
$\Sigma X_i^2 = 2.035$

Substituting into the equation for A and B:

$$A = \frac{3 \Sigma X_i T_i - (\Sigma X_i)(\Sigma T_i)}{3 \Sigma X_i^2 - (\Sigma X_i)^2}$$

$$A = \frac{3\ (527.84) - (2.150)(752.61)}{3(2.035) - (4.622)} = \frac{-34.59}{1.483} = -23.32$$

$$B = \frac{(\Sigma T_i)(\Sigma X_i^2) - (\Sigma X_i T_i)(\Sigma X_i)}{3 \Sigma X_i^2 - (\Sigma X_i)^2}$$

$$B = \frac{(752.61)(2.035) - (527.84)(2.150)}{3(2.035) - 4.622} = \frac{396.71}{1.483} = 267.505$$

Substituting into the original equation:

$T = -23.32X + 267.50$

and solving for the temperature at the surface (X = 1.710)

$T_w = 227.62°F$

c) $T_w - T_{sat}$ determined from: ex. Run 16 - Data Point 3

227.62 - 212.13 = 15.60°F

d) Thermal Conductivity - An equation for the thermal conductivity as a function of the temperature was obtained from the following data for Nickel 200 (formerly Nickel "A") [18] utilizing again the Least Squares Polynomial Fitting Subroutine for a power series:

$$k(T_{av}) = A + BT + CT^2$$

$k(T_{av})$ = thermal conductivity at temperature T

Thermal Conductivity of Nickel "A"

$T^{\circ}F$	$k\left(\frac{Btu}{Hr - Ft - {}^{\circ}F}\right)$
32	42.1
212	37.5
392	33.4
592	29.0

The coefficients obtained resulted in the following equation:

$$k(T_{av}) = 42.8652 - .0241952T_{av} + .0000000077T_{av}^2$$

Where T_{av} is the average temperature over the interval

$$\frac{(T_1 + T_2 + T_{3av})}{3}$$

ex. Run 16 - Data Point 3 ($T_{av} = 250.87$)

$$k(T_{av}) = 42.8652 - .0241952(250.87) + .0000000077(250.87)^2$$

$k(T_{av}) = 36.80$ Btu/Hr - Ft - °F

e) Calculations of Heat Flux from Power Input:

$$\left(\frac{Q}{A}\right)_P = \text{Voltage X Current X } \frac{3.413 \text{ Btu}}{\text{Hr - WATT}} \text{ X } \frac{4}{\pi D^2 Ft^2}$$

ex. Run 16 - Data Point 3 - 27.5 Volts, 3.20 Amps

$$\left(\frac{Q}{A}\right)_P = \frac{27.5 \text{ X } 3.20 \text{ X } 3.413}{0.019} = 15{,}807.57 \text{ Btu/Hr - Ft}^2$$

f) Calculation of Heat Flux from Temperature Profile:

$$\left(\frac{Q}{A}\right)_T = \frac{k(T_1 - T_{3Av})}{(X_3 - X_1)}$$

ex. Run 16 - Data Point 3

$$\left(\frac{Q}{A}\right)_T = \frac{36.80(262.16 - 238.99)°F \text{ X } 12in}{(Hr\text{-}Ft\text{-}°F) \text{ X } .995 \text{ in X Ft}} = 10{,}283.29 \text{ Btu/Hr-Ft}^2$$

3. Heat Transfer Coefficient was Determined from the Equation:

$$h = \frac{(Q/A)_{T\text{-}av}}{T_w - T_{sat}}$$

where $(Q/A)_{T\text{-}av}$ = average heat flux determined from the temperature profile during an experimental run.

$$\left(\frac{Q}{A}\right)_{T\text{-}av} = \left(\sum_{1}^{n} (Q/A)_T\right) / n$$

n = No. of data points in a given run.

ex. Run 14 - Data Point 1

$$\left(\frac{Q}{A}\right)_{T\text{-}av} = 14{,}200$$

$$\Delta T = T_w - T_{sat} = 22.91$$

$$h = \frac{14{,}200}{22.91} = 620 \quad \text{Btu/Hr - Ft}^2 \text{ °F}$$

APPENDIX C

UNCERTAINTY ANALYSIS

In order to check the reliability of the data collected and to determine the magnitude of the most probable error an uncertainty analysis was performed utilizing the method of Kline and McClintock [19].

A. Uncertainty of Measuring Distances:

1. Thermocouple positions = $\pm$ 0.0004 Ft

$$\Delta X = X_1 - X_3$$

$$w_{\Delta X} = \sqrt{w_{X_1}^2 + w_{X_3}^2} = \sqrt{2 \text{ X } .00000016} = .00057\text{Ft}$$

2. Liquid Level:

Low Heat Flux-- $Q/A \leq 15{,}000$ Btu/Hr-Ft^2

$$w_{LL} = \pm .0005 \text{ Ft}$$

Medium-Low Heat Flux-- $15{,}000 \text{ Btu/Hr-Ft}^2 \leq Q/A \leq 25{,}000 \text{ Btu/Hr-Ft}^2$

$$w_{LL} = \pm .0012 \text{ Ft}$$

Medium Heat Flux-- $25{,}000 \text{ Btu/Hr-Ft}^2 \leq Q/A \leq 60{,}000 \text{ Btu/Hr-Ft}^2$

$$w_{LL} = \pm .0030 \text{ Ft}$$

B. Uncertainty in determining heat flux from temperature profile:

$$\frac{Q}{A} = \frac{k \, \Delta T_X}{\Delta X}$$

where k = conductivity, Btu/Hr-Ft °F

$$\Delta T_X = T_1 - T_{3av} \text{ , °F}$$

$$\Delta X = X_1 - X_3 \text{ , Ft}$$

1. Uncertainty in temperature from calibration curves is $\pm$ 0.2°C from Table 9 in Reference [16].

$w_T = \pm .36°F$

2. Uncertainty in T_{3av} - the average temperature of the 4 thermocouples located in position X_3.

$$T_{3av} = \frac{T_a + T_b + T_c + T_d}{4}$$

$$w_{T_a} = w_{T_b} = w_{T_c} = w_{T_d} = \pm .36 \ °F$$

$$\frac{\partial T_{3av}}{\partial T_a} = \frac{\partial T_{3av}}{\partial T_b} = \frac{\partial T_{3av}}{\partial T_c} = \frac{\partial T_{3av}}{\partial T_d} = \frac{1}{4}$$

$$w_{T_{3av}} = \sqrt{\left(\frac{1}{4} w_{T_a}\right)^2 + \left(\frac{1}{4} w_{T_b}\right)^2 + \left(\frac{1}{4} w_{T_c}\right)^2 + \left(\frac{1}{4} w_{T_d}\right)^2}$$

$$w_{T_{3av}} = \sqrt{4\left(\frac{1}{4} w_{T_a}\right)^2} = \frac{2}{4} \sqrt{w_{T_a}^2}$$

$$w_{T_{3av}} = \frac{1}{2} w_{T_a} = \frac{1}{2} (.36) = \pm .18 \ °F$$

3. Uncertainty in $(T_1 - T_{3av})$:

$$\Delta T_X = T_1 - T_{3av}$$

$$\frac{\partial \Delta T_X}{\partial T_1} = 1 \qquad \frac{\partial \Delta T_X}{\partial T_{3av}} = -1$$

$$w_{T_X} = \sqrt{(w_{T_1})^2 + (-w_{T_{3av}})^2} = \sqrt{(.36)^2 + (-.18)^2}$$

$$= \pm .40 \ °F$$

4. Uncertainty in average temperature of the Nickel cylinder for determining conductivity:

$$T_{av} = \frac{T_1 + T_2 + T_{3av}}{3}$$

$$\frac{\partial T_{av}}{\partial T_1} = \frac{\partial T_{av}}{\partial T_2} = \frac{\partial T_{av}}{\partial T_{3av}} = \frac{1}{3}$$

$$w_{T_L} = w_{T_2} = 2w_{T_{3av}}$$

$$w_{T_{av}} = \sqrt{\frac{2}{9} w_{T_1}^2 + \left(\frac{1}{3} w_{T_{3av}}\right)^2} = \sqrt{\frac{2}{9}(.36)^2 + \left(\frac{.18}{3}\right)^2}$$

$$= \pm .18 \text{ °F}$$

5. Uncertainty in determining conductivity-- k:

$$k(T_{av}) = 42.8652 - .0241952\, T_{av} + .0000000077\, (T_{av})^2$$

$$\frac{\partial k}{\partial T_{av}} = -.0241952 + 2(.0000000077)(T_{av})$$

ex. Run 16 Data Point #3; $T_{av} = 250.87$

$$\frac{\partial k}{\partial T_{av}} = -.0241952 + 2(.0000000077)(250.87)$$

$$= .024$$

$$w_k = \sqrt{\left(\frac{\partial k}{\partial T_{av}} w_{T_{av}}\right)^2} = \frac{\partial k}{\partial T_{av}} w_{T_{av}}$$

$$= (.024)(.18) = \pm .004 \text{ Btu/Hr-Ft °F}$$

The above uncertainty in conductivity was determined from the equation for $k(T_{av})$ above. The data from which this equation was formed, using the least squares polynomial curve fitting technique, was believed to have an uncertainty of $\pm$ 1% which is considerably larger than the uncertainty given above; therefore, the actual uncertainty in $k(T_{av})$ was assumed to be:

$$w_k = \pm 0.4 \text{ Btu/Hr-Ft } ^\circ\text{F}$$

6. Uncertainty in heat flux:

let $Q = \frac{Q}{A}$

$$Q = \frac{k \Delta T_X}{\Delta X}$$

$$\frac{\partial Q}{\partial k} = \frac{\Delta T_X}{\Delta X} = \frac{24.18}{.0829} = 291.68$$

$$\frac{\partial Q}{\partial \Delta T_X} = \frac{k}{\Delta X} = \frac{36.80}{.0829} = 443.91$$

$$\frac{\partial Q}{\partial \Delta X} = \frac{-k \Delta T_X}{\Delta X^2} = \frac{-(36.80)(24.18)}{(.0829)^2} = -129477.72$$

$$w_Q = \left[\left(\frac{\partial Q}{\partial k} w_k \right)^2 + \left(\frac{\partial Q}{\partial \Delta T_X} w_{\Delta T_X} \right)^2 + \left(\frac{\partial Q}{\partial \Delta X} w_{\Delta X} \right)^2 \right]^{\frac{1}{2}}$$

$$w_Q = \left[(291.68 \text{ X } .4)^2 + (443.91 \text{ X } .40)^2 + (-129477.72 \text{ X } .00057)^2 \right]^{\frac{1}{2}}$$

$$w_Q = \pm 224.71 \text{ Btu/Hr-Ft}^2$$

C. Uncertainty in $\Delta T = T_w - T_{sat}$:

1. Uncertainty in surface temperature - T_w:

$$\frac{Q}{A} = \frac{k \Delta T_0}{\Delta X_0}$$

where $\Delta X_0 = X_4 - X_3$

$\Delta T_0 = T_{3av} - T_w$

$$\therefore T_w = T_{3av} - \frac{\Delta X_0}{k} \left(\frac{Q}{A}\right)$$

let $Q = \frac{Q}{A}$

$$T_w = T_{3av} - \frac{\Delta X_o}{k} Q$$

ex. Run 16 Data Point 3

$$\frac{\partial T_w}{\partial T_{3av}} = 1$$

$$\frac{\partial T_w}{\partial \Delta X_o} = -\frac{Q}{k} = \frac{-10,284}{36.80} = -279.46$$

$$\frac{\partial T_w}{\partial k} = \frac{\Delta X_o Q}{k^2} = \frac{(.495/12)(10284)}{(36.80)^2} = .31$$

$$\frac{\partial T_w}{\partial Q} = \frac{-\Delta X_o}{k} = -\frac{.495}{(12)(36.8)} = -.0011$$

$$w_{T_w} = \left[\left(\frac{\partial T_w}{\partial T_{3av}} w_{T_{3av}} \right)^2 + \left(\frac{\partial T_w}{\partial \Delta X_o} w_{\Delta X_o} \right)^2 + \left(\frac{\partial T_w}{\partial Q} w_Q \right)^2 + \left(\frac{\partial T_w}{\partial k} w_k \right)^2 \right]^{\frac{1}{2}}$$

$$w_{T_w} = (.18)^2 + (-279.46 \times .00057)^2 + (-.0011 \times 224.71)^2 + (.31 \times .4)^2 \quad \frac{1}{2}$$

$$w_{T_w} = \pm .37 \ ^\circ F$$

2. Uncertainty in pressure readings from aneroid barometer;

$w_p = \pm .5$ mm Hg

3. Uncertainty in determining saturation temperature:

$$T_{sat} = 100 = 28.012 \left(\frac{P}{P_o} - 1\right) - 11.64\left(\frac{P}{P_o} - 1\right)^2 + 7.1 \left(\frac{P}{P_o} - 1\right)^3$$

$$\frac{\partial T_{sat}}{\partial P} = \frac{28.012}{P_o} - 23.28 \left(\frac{P}{P_o} - 1\right)\left(\frac{1}{P_o}\right) + 21.3 \left(\frac{P}{P_o} - 1\right)^2\left(\frac{1}{P_o}\right)$$

ex. Run 16 P=761.9 mm Hg

$$\frac{\partial T_{sat}}{\partial P} = .04$$

$$w_{T_{sat}} = \frac{\partial T_{sat}}{\partial P} w_p = (.04)(0.5) = \pm .02°C$$

$$= \pm .04 \ °F$$

4. Uncertainty in $\Delta T = T_w - T_{sat}$

$$\frac{\partial \Delta T}{\partial T_w} = 1 \qquad \frac{\partial \Delta T}{\partial T_{sat}} = -1$$

$$w_{\Delta T} = \sqrt{(w_{T_w})^2 + (-w_{T_{sat}})^2} = \sqrt{(.37)^2 + (-.04)^2}$$

$$= \pm .37 \ °F$$

D. Uncertainty in heat transfer coefficient:

ex. Run 16 Data Point #3

$$h = \frac{k \ \Delta T_X}{(\Delta X)(\Delta T)}$$

$$\frac{\partial h}{\partial \Delta T_X} = \frac{k}{(\Delta X)(\Delta T)} = \frac{36.80}{(15.60)(.0829)} = 28.46$$

$$\frac{\partial h}{\partial \Delta X} = \frac{-k \ \Delta T_X}{(\Delta T)(\Delta X)^2} = \frac{-36.80(24.18)}{15.60(.0829)^2} = -8299.85$$

$$\frac{\partial h}{\partial \Delta T} = \frac{-k \ \Delta T_X}{\Delta X(\Delta T)^2} = \frac{-36.80(24.18)}{.0829 \ (15.60)^2} = -44.11$$

$$\frac{\partial h}{\partial k} = \frac{\Delta T_X}{\Delta X(\Delta T)} = \frac{24.18}{.0829(15.60)} = 18.70$$

$$w_h = \left[\left(\frac{\partial h}{\partial \Delta X} w_{\Delta X} \right)^2 + \left(\frac{\partial h}{\partial \Delta T} w_{\Delta T} \right)^2 + \left(\frac{\partial h}{\partial k} w_k \right)^2 + \left(\frac{\partial h}{\partial \Delta T_X} w_{\Delta T_X} \right)^2 \right]^{\frac{1}{2}}$$

$$w_h = \left[(-8299.85 \times .00057)^2 + (-44.11 \times .32)^2 + (18.70 \times .4)^2 + (28.46 \times .40)^2 \right]^{\frac{1}{2}}$$

$$= \pm 20.18 \text{ Btu/Hr-Ft}^2 \text{ °F}$$

E. Uncertainty at a higher heat flux:

ex. Run 16 Data Point 5

$\frac{Q}{A} = 14{,}412 \text{ Btu/Hr-Ft}^2$

$\Delta T = 23.93$ °F

$T_{3av} = 252.35$ °F

$\Delta T_X = 32.87$ °F

$T_{av} = 268.87$ °F

$k = 36.36 \text{ Btu/Hr-Ft}^2 \text{ °F}$

$w_k = \pm .4 \text{ Btu/Hr-Ft}^2 \text{ °F}$

$w_Q = \pm 234.04 \text{ Btu/Hr-Ft}^2$

$w_{T_w} = \pm .40$ °F

$w_{\Delta T} = \pm .40$ °F

$w_h = \pm 20.93 \text{ Btu/Hr-Ft}^2 \text{ °F}$

APPENDIX D

LEAST SQUARE METHOD FOR OBTAINING SURFACE TEMPERATURE

Figure 21 is a plot of the temperature distribution within the nickel test cylinder at various power inputs. As shown the temperature profile appears to be linear, and the surface temperature (temperature at point 0.0) could easily be determined by extending a line through the plotted points to the surface; however, this would have been a time-consuming process and another method was desirable. The linearity of the temperature profile provided an opportunity to obtain a functional relationship for the surface temperature by using the method of least squares as described by Holman [20]. An equation of the form:

$$T = AX + B$$

was required to obtain T_w, where the constants A and B were determined from the equations:

$$A = \frac{3\Sigma X_i T_i - (\Sigma X_i)(\Sigma T_i)}{3\Sigma X_i^2 - (\Sigma X_i)^2}$$

$$B = \frac{(\Sigma T_i)(\Sigma X_i^2) - (\Sigma X_i T_i)(\Sigma X_i)}{3\Sigma X_i^2 - (\Sigma X_i)^2}$$

where i = 1, 2, and 3

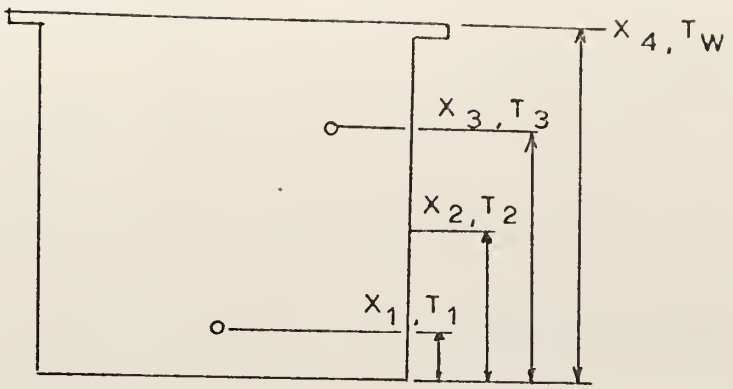

With the axis of the coordinate system at the bottom of the nickel cylinder, the following values were determined by the measurement of thermocouple position, and surface height.

Test Cylinder #1	Test Cylinder #2
X_1 = 0.220 in.	X_1 = 0.200 in.
X_2 = 0.715 in.	X_2 = 0.705 in.
X_3 = 1.215 in.	X_3 = 1.205 in.
X_4 = 1.710 in.	X_4 = 1.690 in.

With the constants determined for a given temperature profile and the distance to the surface known, the surface temperature, T_w, was easily determined as shown in Appendix B.

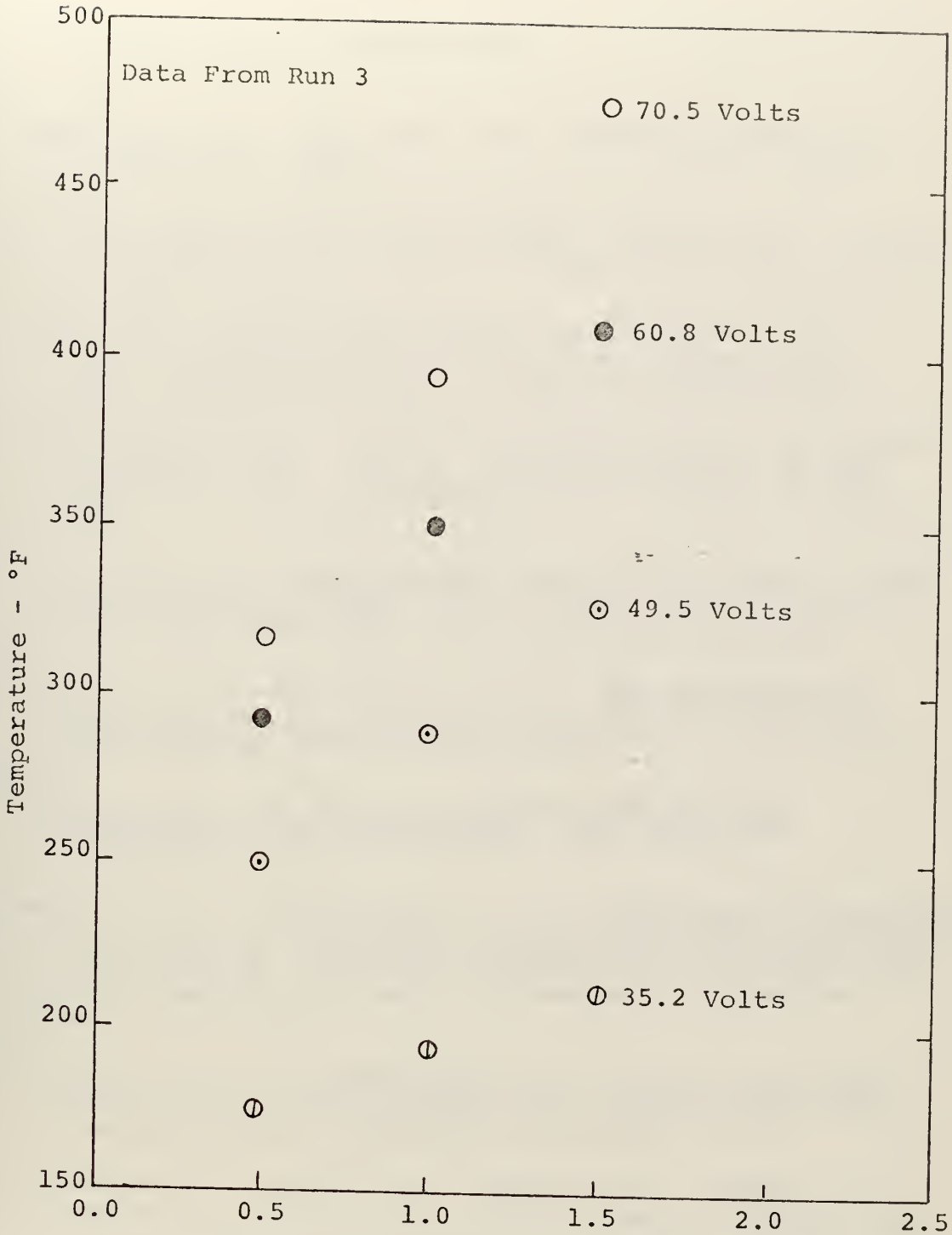

Figure 21. Temperature Profile in Nickel Cylinder

BIBLIOGRAPHY

1. Eastman, G. Y., "The Heat Pipe," Scientific American, p. 38-46, May 1968.

2. Grover, G. M., Cotter, T. P. and Erickson, G. F., "Structures of Very High Thermal Conductance," Journal of Applied Physics, v. 35, p. 1990-1991, 1964.

3. Naval Civil Engineering Laboratory Technical Note N-1207, Investigation of Heat Pipe Technology for Naval Application, by S. C. Garg, February 1972.

4. Lawrence Radiation Laboratory, University of California, Livermore, UCRL - 50453, A Critical Review of Heat Pipe Theory and Applications, by H. Cheung, 15 July 1968.

5. Alleavitch, J., Vaporization Heat Transfer From Flooded Wick Covered Surfaces, Ph.D. Thesis, North Carolina State University, Raleigh, North Carolina, 1969.

6. Ferrell, J. K. and Johnson, H. R., The Mechanism of Heat Transfer in the Evaporator Zone of a Heat Pipe, ASME Preprint 70-HT/SpT-12, 1970.

7. Seban, R. A. and Abhat, A., Steady and Maximum Evaporation From Screen Wicks, ASME Paper No. 71-WA/HT-12, 1971

8. Marto, P. J. and Mosteller, W. L., The Effect of Nucleate Boiling on the Operation of Low Temperature Heat Pipes, ASME Paper No. 69-HT-24, presented at the ASME-AIChE Heat Transfer Conference, Minneapolis, Minnesota, August 3-6, 1969.

9. Gregory, F. C., An Investigation of Nucleate Boiling From Mesh Covered Surfaces, M.S. Thesis, Naval Postgraduate School, Monterey, California, 1970.

10. Nishikawa, K., Kusuda, H., Yamasaki, K., Tanaka, K., "Nucleate Boiling at Low Liquid Levels," Trans. Japan Society of Mechanical Engineers, v. 10, No. 38, p. 328-38, 1967.

11. Patten, T. D. and Turmeau, W. A., "Some Characteristics of Nucleate Boiling in Thin Liquid Layers," Heat Transfer 1970, V. V, Paper No. B 2.10, 1970.

12. Lewis Research Center, NASA CR-812, Vapor-Chamber Fin Studies, Transport Properties and Boiling Characteristics of Wicks, by H. R. Kunz, L. S. Langston, B. H. Hilton, S. S. Wyde, and G. H. Nashick, June 1967.

13. Massachusetts Institute of Technology Report 5219-23, The Effect of Surface Conditions on Nucleate Pool Boiling Heat Transfer to Sodium, by P. J. Marto and W. M. Rohsenow, p. 42, January 1965.

14. Rohsenow, W. M., and Choi, H. Y., Heat, Mass and Momentum Transfer, p. 225, Prentice-Hall, Englewood Cliffs, New Jersey, 1961.

15. Johnson, B. M., Jansen, G. and Owzarski, P. C., Enhanced Evaporating Film Heat Transfer From Corrugated Surfaces, ASME Paper No. 71-HT-33, 1971.

16. United States Department of Commerce, National Bureau of Standards Circular 590, Methods of Testing Thermocouples and Thermocouple Materials, by Wm. F. Roeser and S. T. Lonberger, 6 February 1958.

17. Van Vlack, L. H., Elements of Material Science, p. 190, Addison-Wesley, 1959.

18. Hogan & Sawyer, Journal of Applied Physics, 23, 177 (1952).

19. Kline, S. J. and McClintock, F. A., "Describing Uncertainties in Single-Sample Experiments," Mechanical Engineering, v. 75, p. 3-8, January 1953.

20. Holman, J. P., Experimental Methods for Engineers, p. 37-40, p. 61-64, McGraw-Hill, New York, 1966.

INITIAL DISTRIBUTION LIST

		No. Copies
1.	Defense Documentation Center Cameron Station Alexandria, Virginia 22314	2
2.	Library, Code 0212 Naval Postgraduate School Monterey, California 93940	2
3.	Assoc. Professor P. J. Marto, Code 59Mx Department of Mechanical Engineering Naval Postgraduate School Monterey, California 93940	1
4.	Professor P. F. Pucci, Code 59Pc Department of Mechanical Engineering Naval Postgraduate School Monterey, California 93940	1
5.	Mr. Robert H. Chapman Oak Ridge National Laboratory P. O. Box Y Oak Ridge, Tennessee 37830	1
6.	LT Donald Kenneth MacKenzie, USN c/o The Marshalls 40 Forest Lane Swarthmore, Pennsylvaina 19081	1
7.	Mechanical Engineering Department Library Code 59 Naval Postgraduate School Monterey, California 93940	1

Security Classification

DOCUMENT CONTROL DATA - R & D

(Security classification of title, body of abstract and indexing annotation must be entered when the overall report is classified)

ORIGINATING ACTIVITY (Corporate author)

Naval Postgraduate School
Monterey, California 93940

2a. REPORT SECURITY CLASSIFICATION
Unclassified

2b. GROUP

REPORT TITLE

Vaporization of Thin Liquid Films

DESCRIPTIVE NOTES (Type of report and inclusive dates)

Master's Thesis; December 1972

AUTHOR(S) (First name, middle initial, last name)

Donald Kenneth MacKenzie

REPORT DATE	7a. TOTAL NO. OF PAGES	7b. NO. OF REFS
December 1972	91	20

CONTRACT OR GRANT NO.

PROJECT NO.

9a. ORIGINATOR'S REPORT NUMBER(S)

9b. OTHER REPORT NO(S) (Any other numbers that may be assigned this report)

DISTRIBUTION STATEMENT

Approved for public release; distribution unlimited.

SUPPLEMENTARY NOTES

12. SPONSORING MILITARY ACTIVITY

Naval Postgraduate School
Monterey, California

ABSTRACT

Experimental results are presented for saturated nucleate pool boiling of distilled water and ethyl-alcohol from 1-7/8" diameter Nickel disks with pool depths from 1.0 inch to a thin film of 0.015 inch. Experimental runs were conducted on a mirrorlike surface utilizing distilled water and ethyl-alcohol; on a grooved surface with distilled water as the working fluid; and on a surface covered with 4 layers of Nickel 50 x 40 mesh with distilled water as the working fluid.

Results show that liquid level has little effect on the heat transfer coefficient above a level of 0.2 inch on all three test surfaces; however, below 0.2 inch a rapid increase in the heat transfer coefficient occurs with the lowering of the liquid level. Two types of thin film dryout were noted on the mirrorlike surface: dryout under a dome and dryout in absence of a dome. A grooved surface appears to provide a means of obtaining a stable high heat transfer coefficient at liquid films as thin as 0.015 inch.

DD FORM 1 NOV 65 1473 (PAGE 1)

S/N 0101-807-6811

UNCLASSIFIED
Security Classification

A-31408

KEY WORDS	LINK A		LINK B		LINK C	
	ROLE	WT	ROLE	WT	ROLE	WT
Nucleate Boiling						
Thin Films						
Vaporization						

13 DEC 73
28 MAY 76
3 SEP 76
21833
23550
23356

141393
Thesis
M2235 MacKenzie
c.1 Vaporization of thin liquid films.